J. Fluid Mech. (2001), *vol.* 432, *pp.* 167–200. Printed in the United Kingdom

© 2001 Cambridge University Press

An adaptive multimodal approach to nonlinear sloshing in a rectangular tank

By ODD M. FALTINSEN[1] AND ALEXANDER N. TIMOKHA[2]

[1]Department of Marine Hydrodynamics, Faculty of Marine Technology, NTNU, Trondheim, N-7491, Norway

[2]Institute of Mathematics, National Academy of Sciences of Ukraine, Tereschenkivska, 3 str., Kiev, 252601, Ukraine

(Received 4 January 2000 and in revised form 23 August 2000)

Two-dimensional nonlinear sloshing of an incompressible fluid with irrotational flow in a rectangular tank is analysed by a modal theory. Infinite tank roof height and no overturning waves are assumed. The modal theory is based on an infinite-dimensional system of nonlinear ordinary differential equations coupling generalized coordinates of the free surface and fluid motion associated with the amplitude response of natural modes. This modal system is asymptotically reduced to an infinite-dimensional system of ordinary differential equations with fifth-order polynomial nonlinearity by assuming sufficiently small fluid motion relative to fluid depth and tank breadth. When introducing inter-modal ordering, the system can be detuned and truncated to describe resonant sloshing in different domains of the excitation period. Resonant sloshing due to surge and pitch sinusoidal excitation of the primary mode is considered. By assuming that each mode has only one main harmonic an adaptive procedure is proposed to describe direct and secondary resonant responses when Moiseyev-like relations do not agree with experiments, i.e. when the excitation amplitude is not very small, and the fluid depth is close to the critical depth or small. Adaptive procedures have been established for a wide range of excitation periods as long as the mean fluid depth h is larger than 0.24 times the tank breadth l. Steady-state results for wave elevation, horizontal force and pitch moment are experimentally validated except when heavy roof impact occurs. The analysis of small depth requires that many modes have primary order and that each mode may have more than one main harmonic. This is illustrated by an example for $h/l = 0.173$, where the previous model by Faltinsen *et al.* (2000) failed. The new model agrees well with experiments.

1. Introduction

A partially filled tank in a ship can experience violent fluid cargo loads. The model of 'frozen' fluid and linear theory of sloshing are not applicable in this case. Very long time simulations are needed to obtain statistical estimates of the fluid cargo response. Complex transients should be accounted for. Examples of direct numerical simulations of the fluid motions in a tank have been reported by Moan & Berge (1997), and EUROSLOSH Report (1995). These methods use various finite-difference, finite-element and boundary-element approaches but it is difficult to perform long time simulations. One reason is problems in satisfying volume (energy) conservation in long time simulations, which then give non-realistic flows. There is

https://doi.org/10.1017/S0022112000003311 Published online by Cambridge University Press

also the additional problem of describing accurately fluid impact inside the tank (see Faltinsen & Rognebakke 2000).

Several analytical approaches based on potential theory have been developed to study nonlinear sloshing. Most of them examine the fluid response to regular harmonic longitudinal or parametric excitations and use a combined asymptotic and modal technique. In a modal representation Fourier series with time-dependent coefficients (generalized coordinates) are used to describe the free surface evolution. The surface shape is expressed mathematically as

$$z = f(x, y, t) = \sum_{i=1}^{\infty} \beta_i(t) f_i(x, y), \tag{1.1}$$

where the $Oxyz$ coordinate system is fixed relative to the tank and t is time. The set of functions $\{f_i(x, y): \int_{\Sigma_0} f_i \, \mathrm{d}S = 0\}$ is a Fourier basis for the mean free surface Σ_0 satisfying the volume conservation condition. Spectral theorems of linear sloshing (proved for instance in Feschenko *et al.* 1969) show that a suitable Fourier basis is the set of natural modes. There is a limited class of tank shapes where analytical solutions of the natural modes are known. Examples are two- or three-dimensional rectangular tanks and vertical circular cylindrical tanks. Otherwise, numerical methods have to be used to find surface mode shapes as was done by Solaas & Faltinsen (1997). The expansion of the solution in a series of eigenfunctions is convenient when sloshing resembles standing waves, namely for finite fluid depth. It is not convenient when travelling waves matter, i.e. for smaller fluid depth.

If it is assumed that the generalized coordinates $\beta_i(t)$ are sufficiently small within the known asymptotic inter-modal relationship, the modal presentation (1.1) becomes the base for an asymptotic approach. It reduces the original free boundary problem to a finite sequence of asymptotic approximations in β_i. The asymptotic procedure implies typically a single dominant function β_k so that $1 \gg \beta_k \gg \beta_i,\ i \geqslant 1, i \neq k$. An appropriate inter-modal relationship (detuning procedure) with one dominating primary mode β_1 was proposed by Moiseyev (1958) to describe steady-state (periodic) resonant sloshing in a two-dimensional rectangular tank. The tank was forced to oscillate horizontally and sinusoidally with small amplitude in a frequency domain close to the lowest natural frequency. This made it possible to develop the third-order theory of steady-state sloshing due to small-amplitude horizontal (angular) excitation reported by Faltinsen (1974). This theory is not uniformly valid for critical depth $h/l = 0.3374\ldots$ (l is the tank breadth). The fifth-order fluid response at critical depth was derived by Waterhouse (1994) in order to cover this case. Moiseyev's detuning procedure undergoes a change for small fluid depths. This was reported by for instance Ockendon, Ockendon & Johnson (1986).

The single dominant asymptotic relations introduced by Moiseyev have also been used to describe the modulated (unsteady) waves in a two-dimensional rectangular tank. A Duffing-like equation describes the slowly varying primary mode amplitude $\langle\beta_1\rangle$. The derivations of this equation can be found for instance in papers by Shemer (1990) and Tsai, Yue & Yip (1990). The Moiseyev-like approach was extended to three-dimensional vertical cylindrical tanks of rectangular (circular) cross-sections by Miles (1984*a*, *b*, 1994), and Henderson & Miles (1991) for both directly and parametrically excited surface waves.

Non-dominating modes have also been accounted for. For instance, Faltinsen (1974) and Faltinsen *et al.* (2000) have considered the contribution of the second and third (driven) modes for respectively steady-state and unsteady sloshing. Faltinsen *et al.*

https://doi.org/10.1017/S0022112000003311 Published online by Cambridge University Press

(2000) derived a modal system of nonlinear ordinary differential equations coupling nonlinearly β_1, β_2 and β_3. This modal system is consistent with Moiseyev's asymptotic assumptions and implies $\beta_1 \sim \epsilon^{1/3}$, $\beta_2 \sim \epsilon^{2/3}$, $\beta_3 \sim \epsilon$, where ϵ is small parameter characterizing the ratio between the excitation amplitude and the tank breadth. This modal system was validated for different finite fluid depths, excitation periods and small excitation amplitudes by experimental studies of sway (surge) sinusoidally excited sloshing. Time records of wave elevation near the wall starting from an initially calm fluid up to a time corresponding to 50 forced oscillation periods were studied. It was shown that the second and third modes contribute considerably. Beating waves due to nonlinear interactions between natural and forced solutions were important for a very long time. Steady-state solutions, where the beating disappears, were not achieved during the time period examined for the cases studied without tank roof impact. The reason is the very small damping in smooth tanks as long as the water does not hit the tank roof. Good agreement between theory and experiment was documented.

Further investigations by this asymptotic model have shown its limitations in simulating fluid sloshing when maximum free surface elevation is the order of the tank breadth or fluid depth. This happens if either ϵ is not very small, or the depth h is close to the critical value $h/l = 0.3374\ldots$ or in shallow water. The numerical simulations give a non-realistic response in the secondary modes. The assumption of a single dominant mode is then questionable. A way to solve this problem for surge- and pitch-excited sloshing in a rectangular tank is proposed in this paper. The failure of the asymptotic approximations is explained as due to nonlinear fluid interactions causing energy with frequency content at higher natural frequencies. The analysis is based on the concept of the secondary resonance predicted for steady-state solutions by Faltinsen *et al.* (2000). It suggests that for resonance harmonic excitation of the primary mode (σ is the excitation frequency and $\sigma \to \sigma_1$)† nonlinearities can cause oscillations with frequency $m\sigma$ so that the mth natural frequency σ_m of the fluid is close to $m\sigma$. The generalized coordinate β_m will be amplified and can be of the same order as β_1. Since the difference between natural frequencies decreases with decreasing fluid depth, this is more likely to occur at smaller fluid depths. This is a reason why the single dominant mode theories are invalid for small fluid depth. In addition, if the excitation amplitude increases, the fluid response becomes large in an increased frequency domain around the primary natural frequency. The effective domain of the secondary resonance increases too. The second and third mode secondary resonance zones can overlap with the primary resonant zone and each other. Since the amplification of the fluid motion is relatively larger in the vicinity of the critical depth than at other fluid depths, the upper bound of tank excitation amplitude where the theory by Faltinsen *et al.* (2000) is applicable for critical depth is relatively small.

We will still assume ϵ to be small and that the response is asymptotically larger than the excitation. The method uses the infinite-dimensional nonlinear modal system derived by Faltinsen *et al.* (2000) and Taylor expansion of volume-varying integrals depending on β_i. The derived approximate modal system couples β_i and translatory body motion terms up to fifth-order polynomials in β_i. Third-order terms are included for angular excitation. The procedure is consistent with asymptotic assumptions by Narimanov (1957). The coefficients of this system depend uniquely on the mean depth, and can be computed before a time simulation. This infinite-dimensional

† All the frequencies herein mean circular frequencies with dimension [rad s^{-1}].

https://doi.org/10.1017/S0022112000003311 Published online by Cambridge University Press

system should be detuned (truncated) to obtain a finite-dimensional structure. The Moiseyev asymptotics by Faltinsen *et al.* (2000) is a particular case. The secondary resonance needs two or more modes to have the same order.

The theory is validated by experimental data obtained by Olsen & Johnsen (1975), Olsen (1970, personal communication), Abramson *et al.* (1974) and Mikelis, Miller & Taylor (1984). Comparisons are made for steady-state wave amplitude, hydrodynamic force and moment on the tank. Some isolated cases of transients are considered for small fluid depth. Comparisons are made with experimental time records of wave elevation by Rognebakke (1999). When the mean fluid depth was less than 0.24 times the tank breadth, it was not possible to find asymptotic relations between β_i that applied for all forced excitation periods near primary resonance.

Our Fourier representation prevents us extending the proposed method to travelling and run-up wave phenomena. If it has a finite number of dominant modes, the Fourier series (1.1) can be asymptotically truncated. Both the travelling wave and run-up need an infinite or too large a number of Fourier approximations to get satisfactory convergence. In addition, the series (1.1) has only weak convergence in mean square metrics. The surface modes based on our theory have a right-angled contact angle between fluid surface and tank wall, and, therefore, $(\mathrm{d}/\mathrm{d}x)f_i = 0$ at the wall. However, the real surface shape $z = f(x,t)$ can have a non-right-angled contact angle during run-up. This means that there is a non-uniform convergence of (1.1) on the mean free surface $[-l/2, l/2]$, which can be important at smaller fluid depths.

The theory assumes infinite tank roof height, but roof impact is very likely during realistic sloshing in ship tanks. This can be handled for a horizontal or chamfered tank roof in a similar way as done by Faltinsen & Rognebakke (1999) and Rognebakke & Faltinsen (2000). They used the theory by Faltinsen *et al.* (2000) as an ambient flow. If roof impact is included, the proposed adaptive multimodal approach can be applied to sloshing in a smooth rectangular or prismatic tank of a ship in realistic seaways and allows simulation of coupled motions (see Faltinsen & Rognebakke 2000). But a strategy has to be established that accounts for simultaneous excitation frequencies as well as vertical tank motions.

2. Modal sloshing theory

2.1. *Statement of the problem*

The free boundary problem on sloshing of an incompressible fluid with irrotational flow has the following form:

$$\left.\begin{gathered} \Delta\Phi = 0 \quad \text{in } Q(t); \quad \frac{\partial \Phi}{\partial v} = \boldsymbol{v}_0 \cdot \boldsymbol{v} + \boldsymbol{\omega} \cdot [\boldsymbol{r} \times \boldsymbol{v}] \quad \text{on } S(t), \\ \frac{\partial \Phi}{\partial v} = \boldsymbol{v}_0 \cdot \boldsymbol{v} + \boldsymbol{\omega} \cdot [\boldsymbol{r} \times \boldsymbol{v}] - \frac{\xi_t}{|\nabla \xi|} \quad \text{on } \Sigma(t), \\ \frac{\partial \Phi}{\partial t} - \nabla\Phi \cdot (\boldsymbol{v}_0 + \boldsymbol{\omega} \times \boldsymbol{r}) + \tfrac{1}{2}(\nabla\Phi)^2 + U = 0 \quad \text{on } \Sigma(t), \quad \int_{Q(t)} \mathrm{d}Q = \text{const.} \end{gathered}\right\} \tag{2.1}$$

Here $Q(t)$ is the fluid volume, t is time, $\Phi(x,y,z,t)$ is the velocity potential in the fixed reference frame, $\xi(x,y,z,t) = 0$ is the equation of the free surface and v is the outer normal to $Q(t)$. A moving coordinate, $Oxyz$, system fixed with respect to the body is used. $\boldsymbol{v}_0(t)$ is the translatory velocity vector of the origin O, $\boldsymbol{\omega}(t)$ is the rigid body angular velocity vector, $\boldsymbol{r}$ is the position vector relative to O and U is the gravity potential. Further $S(t)$ is the wetted body surface and $\Sigma(t)$ is the free surface. The

https://doi.org/10.1017/S0022112000003311 Published online by Cambridge University Press

second condition on the free surface, $\Sigma(t)$, is the constant pressure requirement, and the second term in that condition arises from the use of a moving coordinate system.

Faltinsen *et al.* (2000) have developed a semi-analytical variational approach to the free boundary problem (2.1). The variational procedure is based on the works by Miles (1976) and Lukovsky (1976). When a rigid smooth tank has a vertical wall near the free surface in its equilibrium position and no overturning wave occurs, the continuum problem is reduced to a discrete conservative mechanical system with infinite degrees of freedom. The method implies that the free surface $z = f(x,t)$ and Φ in two-dimensional flows are expressed as

$$f(x,t) = \beta^i(t) f_i(x); \quad \Phi(x,z,t) = v_{0x}x + v_{0z}z + \omega(t)\Omega(x,z,t) + R^k(t)\varphi_k(x,z), \tag{2.2}$$

where the repeated upper and lower indexes mean summation and $\boldsymbol{v}_0 = \{v_{0x}, 0, v_{0z}\}$, $\boldsymbol{\omega} = \{0, \omega, 0\}$. Further the set $\{f_i(x)\}$ is a Fourier basis for the mean free surface and $\{\varphi_n(x,z)\}$ is a complete set of harmonic functions having zero normal velocity at the tank boundaries. The completeness of the basis functions is assumed in suitable Sobolev metrics defined, for example, by Marti (1986) for the Neumann boundary problem within the Laplace equation. $\Omega(x,z,t)$ is the Stokes–Zhukovsky potential defined by Neumann boundary value problem

$$\Delta\Omega = 0 \quad \text{in } Q(t); \quad \left.\frac{\partial\Omega}{\partial\nu}\right|_{S(t)+\Sigma(t)} = z\nu_1 - x\nu_3, \tag{2.3}$$

where $\boldsymbol{\nu} = \{\nu_1, 0, \nu_3\}$ is the outer normal to $Q(t)$.

The variational procedure gives the following infinite-dimensional system of nonlinear ordinary differential equations coupling β_i and R_n:

$$\frac{\mathrm{d}}{\mathrm{d}t}A_n - A_{nk}R^k = 0, \quad n \geqslant 1; \tag{2.4}$$

$$\dot{R}^n\frac{\partial A_n}{\partial\beta_\mu} + \frac{1}{2}\frac{\partial A_{nk}}{\partial\beta_\mu}R^nR^k + \left[\dot{\omega}\frac{\partial l_\omega}{\partial\beta_\mu} + \omega\frac{\partial l_{\omega t}}{\partial\beta_\mu} - \frac{\mathrm{d}}{\mathrm{d}t}\left(\omega\frac{\partial l_{\omega t}}{\partial\dot{\beta}_\mu}\right)\right]$$

$$+(\dot{v}_{0x} - g_1 + \omega v_{0z})\frac{\partial l_1}{\partial\beta_\mu} + (\dot{v}_{0z} - g_3 - \omega v_{0x})\frac{\partial l_3}{\partial\beta_\mu} - \frac{1}{2}\omega^2\frac{\partial J^1_{22}}{\partial\beta_\mu} = 0, \quad \mu \geqslant 1, \tag{2.5}$$

where g_i are the projections of the gravity acceleration vector and the dot means a time derivative.

A_n, A_{nk}, l_ω, $l_{\omega t}$, l_1, l_3 and J^1_{22} are integrals over the time-dependent domain $Q(t)$, and, therefore, are functions of β_i. Their explicit form is given by Faltinsen *et al.* (2000) as

$$A_n = \rho\int_{Q(t)}\varphi_n\,\mathrm{d}Q, \quad A_{nk} = \rho\int_{Q(t)}\nabla\varphi_n\cdot\nabla\varphi_k\,\mathrm{d}Q, \tag{2.6}$$

$$l_\omega = \rho\int_{Q(t)}\Omega\,\mathrm{d}Q, \quad l_{\omega t} = \rho\int_{Q(t)}\frac{\partial\Omega}{\partial t}\,\mathrm{d}Q, \quad \frac{\partial l_3}{\partial\beta_i} = \rho\int_{\Sigma_0}f_i^2\,\mathrm{d}S\beta_i; \quad \frac{\partial l_1}{\partial\beta_i} = \rho\int_{\Sigma_0}xf_i\,\mathrm{d}S, \tag{2.7}$$

$$J^1_{22} = \rho\int_{Q(t)}\left(z\frac{\partial\Omega}{\partial x} - x\frac{\partial\Omega}{\partial z}\right)\mathrm{d}Q = \rho\int_{S(t)+\Sigma(t)}\Omega\frac{\partial\Omega}{\partial\nu}\,\mathrm{d}S, \tag{2.8}$$

where ρ is fluid density and Σ_0 is the mean free surface.

https://doi.org/10.1017/S0022112000003311 Published online by Cambridge University Press

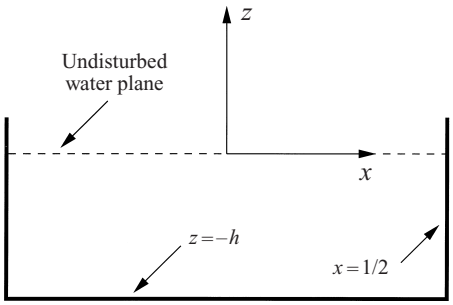


FIGURE 1. Coordinate system.

2.2. *Derivation of third- (fifth)-order modal sloshing theory in a rectangular tank*

We consider the fluid volume $Q(t)$ in a rectangular tank:

$$Q(t) = \{-l/2 < x < l/2, -h < z < f(x,t)\} \tag{2.9}$$

where l is the tank breadth and h is the mean fluid depth. The mean free surface Σ_0 is at $z = 0$ in the moving coordinate system Oxz. The origin O is situated in the middle of the tank (see figure 1).

We associate the modal functions $\{f_i(x)\}$ and $\{\varphi_i(x,z)\}$ with natural modes, i.e.

$$f_i(x) = \cos(\varkappa_i(x + l/2)); \quad \varphi_i(x,z) = f_i(x)\frac{\cosh(\varkappa_i(z+h))}{\cosh(\varkappa_i h)}, \quad \varkappa_i = \frac{\pi i}{l}, \quad i \geqslant 1. \tag{2.10}$$

They can be obtained from the spectral problem for linear sloshing. $f_i(x)$, $i \geqslant 1$ gives the Fourier basis on $(-l/2, l/2)$ in the mean square metric for a square integrable function $f(x) : \int_{-l/2}^{l/2} f(x)\,\mathrm{d}x = 0$. (The last integral condition follows from the volume conservation condition.)

The asymptotic procedure requires Taylor expansions of the integrals (2.6), (2.7) and (2.8) in the Taylor series in β_i and excitation components $\dot{v}_{0x}, \dot{v}_{0z}, \omega$. This is only possible if the resulting free surface elevation with respect to the mean free surface is sufficiently small relative to tank breadth or fluid depth.

The integrals A_n, A_{nk} will be expanded up to fifth-order polynomials in β_i. Other integrals depending on Ω will be expanded up to third order, due to mathematical problems in asymptotic approximations. The zero-order approximation of Ω does not allow for calculations of high derivatives.

The Taylor series of (2.6) gives

$$\frac{A_n}{\rho} = \int_{Q_0} \varphi_n\,\mathrm{d}Q + \int_{-l/2}^{l/2} \varphi_n f\,\mathrm{d}x + \frac{1}{2}\int_{-l/2}^{l/2} \left.\frac{\partial \varphi_n}{\partial z}\right|_{z=0} f^2\,\mathrm{d}x + \frac{1}{6}\int_{-l/2}^{l/2} \left.\frac{\partial^2 \varphi_n}{\partial z^2}\right|_{z=0} f^3\,\mathrm{d}x$$
$$+\frac{1}{24}\int_{-l/2}^{l/2} \left.\frac{\partial^3 \varphi_n}{\partial z^3}\right|_{z=0} f^4\,\mathrm{d}x + \frac{1}{120}\int_{-l/2}^{l/2} \left.\frac{\partial^4 \varphi_n}{\partial z^4}\right|_{z=0} f^5\,\mathrm{d}x + o(f^5). \tag{2.11}$$

By inserting (2.2) into (2.11) we get, correct to fifth order,

$$A_n = \rho\frac{l}{2}\{\beta_n + \tfrac{1}{2}E_n \Lambda^{(1)}_{nij}\beta^i\beta^j + \tfrac{1}{3}C_{nn}\Lambda^{(2)}_{nijk}\beta^i\beta^j\beta^k + \tfrac{1}{12}C_{nn}E_n\Lambda^{(3)}_{nijkp}\beta^i\beta^j\beta^k\beta^p$$
$$+\tfrac{1}{30}C^2_{nn}\Lambda^{(4)}_{nijkpq}\beta^i\beta^j\beta^k\beta^p\beta^q\}, \tag{2.12}$$

https://doi.org/10.1017/S0022112000003311 Published online by Cambridge University Press

where

$$E_n = 0.5\varkappa_n \tanh(\varkappa_n h) = \frac{\pi n}{2l}\tanh(\varkappa_n h); \quad C_{nk} = \tfrac{1}{8}\varkappa_n\varkappa_k = nk\frac{\pi^2}{8l^2}. \tag{2.13}$$

Here we have introduced the integer tensors $\boldsymbol{\Lambda}$, defined in Appendix A. The tensors $\boldsymbol{\Lambda}$ are zero when one of the indexes exceeds the sum of the other indexes (for example, $\Lambda^{(4)}_{nabcdf} = 0$, when $n > a+b+c+d+f$). This leads to *finite tensor sums* in most of the formulas below unless the expressions are based on the other set of tensors $\boldsymbol{X}$ and $\boldsymbol{Y}$ (see their definitions in Appendix A). The *summation symbol* will then be introduced to underline that a sum becomes *infinite*.

Equations (2.4) and (2.5) require $\mathrm{d}A_n/\mathrm{d}t$ and $\partial A_n/\partial\beta_\mu$ to be known. The explicit expressions for these derivatives are

$$\frac{\mathrm{d}A_n}{\mathrm{d}t} = \rho\frac{l}{2}\{\dot\beta_n + E_n\Lambda^{(1)}_{nij}\dot\beta^i\beta^j + C_{nn}\Lambda^{(2)}_{nijk}\dot\beta^i\beta^j\beta^k + \tfrac{1}{3}C_{nn}E_n\Lambda^{(3)}_{nijkp}\dot\beta^i\beta^j\beta^k\beta^p + \tfrac{1}{6}C^2_{nn}\Lambda^{(4)}_{nijkpq}\dot\beta^i\beta^j\beta^k\beta^p\beta^q\}; \tag{2.14}$$

$$\frac{\partial A_n}{\partial\beta_\mu} = \rho\frac{l}{2}\{\delta_{n\mu} + E_n\Lambda^{(1)}_{ni\mu}\beta^i + C_{nn}\Lambda^{(2)}_{nij\mu}\beta^i\beta^j + \tfrac{1}{3}C_{nn}E_n\Lambda^{(n)}_{nijk\mu}\beta^i\beta^j\beta^k + \tfrac{1}{6}C^2_{nn}\Lambda^{(4)}_{nijkp\mu}\beta^i\beta^j\beta^k\beta^p\}. \tag{2.15}$$

The tensor products $A_{nk}R^k$ in (2.4) and $(\partial A_{nk}/\partial\beta_\mu)R^nR^k$ in (2.5) should be calculated up to fifth-order polynomials in R_k. The expansion of A_{nk} must therefore be made up to fourth order. The Taylor series gives

$$\begin{aligned}\frac{A_{nk}}{\rho} = {} & \int_{Q_0}\nabla\varphi_n\cdot\nabla\varphi_k\,\mathrm{d}Q + \int_{-l/2}^{l/2}(\nabla\varphi_n\cdot\nabla\varphi_k)\Big|_{z=0} f\,\mathrm{d}x \\ & + \frac{1}{2}\int_{-l/2}^{l/2}\frac{\partial(\nabla\varphi_n\cdot\nabla\varphi_k)}{\partial z}\Big|_{z=0} f^2\,\mathrm{d}x + \frac{1}{6}\int_{-l/2}^{l/2}\frac{\partial^2(\nabla\varphi_n\cdot\nabla\varphi_k)}{\partial z^2}\Big|_{z=0} f^3\,\mathrm{d}x \\ & + \frac{1}{24}\int_{-l/2}^{l/2}\frac{\partial^3(\nabla\varphi_n\cdot\nabla\varphi_k)}{\partial z^3}\Big|_{z=0} f^4\,\mathrm{d}x + o(f^4).\end{aligned} \tag{2.16}$$

It follows that

$$A_{nk} = \rho\frac{l}{2}(\delta_{nk}2E^k + \Pi^{(1)}_{nk,i}\beta^i + \Pi^{(2)}_{nk,ij}\beta^i\beta^j + \Pi^{(3)}_{nk,ijp}\beta^i\beta^j\beta^p + \Pi^{(4)}_{nk,ijpq}\beta^i\beta^j\beta^p\beta^q), \tag{2.17}$$

where the comma separates symmetric sets of indexes. The tensors Π are

$$\left.\begin{aligned}\Pi^{(1)}_{nk,i} &= 4C_{nk}\Lambda^{(-1)}_{nk,i} + 2E_nE_k\Lambda^{(1)}_{nki},\\ \Pi^{(2)}_{nk,ij} &= 2C_{nk}(E_n+E_k)\Lambda^{(-2)}_{nk,ij} + 2(C_{nn}E_k + C_{kk}E_n)\Lambda^{(2)}_{nkij},\\ \Pi^{(3)}_{nk,ijp} &= \tfrac{2}{3}[2C_{nk}(C_{nn}+C_{kk}+E_kE_n)\Lambda^{(-3)}_{nk,ijp} + (E_nE_k(C_{nn}+C_{kk}) + 4C^2_{nk})\Lambda^{(3)}_{nk,ipq}],\\ \Pi^{(4)}_{nk,ijpq} &= \tfrac{1}{3}[C_{nk}(E_n(C_{nn}+3C_{kk}) + E_k(C_{kk}+3C_{nn}))\Lambda^{(-4)}_{nk,ijpq}\\ &\quad + (E_kC_{nn}(C_{nn}+3C_{kk}) + E_nC_{kk}(C_{kk}+3C_{nn}))\Lambda^{(4)}_{nk,ijpq}].\end{aligned}\right\} \tag{2.18}$$

https://doi.org/10.1017/S0022112000003311 Published online by Cambridge University Press

The partial derivatives of A_{nk} by β_μ have the form

$$\frac{\partial A_{nk}}{\partial \beta_\mu} = \rho \frac{l}{2}[\Pi^{(1)}_{nk,\mu} + 2\Pi^{(2)}_{nk,i\mu}\beta^i + 3\Pi^{(3)}_{nk,ij\mu}\beta^i\beta^j + 4\Pi^{(4)}_{nk,ijp\mu}\beta^i\beta^j\beta^p]. \tag{2.19}$$

Furthermore (2.4) is considered as a linear system of algebraic equations with respect to functions R^k, i.e.

$$A_{nk}R^k = \frac{\mathrm{d}A_n}{\mathrm{d}t}. \tag{2.20}$$

Here R^k can be expressed correct to fifth-order polynomials in β^i and $\dot\beta^i$ as

$$R^k = \frac{\dot\beta^k}{2E_k} + V^{2,k}_{i,j}\dot\beta^i\beta^j + V^{3,k}_{i,j,p}\dot\beta^i\beta^j\beta^p + V^{4,k}_{i,j,p,q}\dot\beta^i\beta^j\beta^p\beta^q + V^{5,k}_{i,j,p,q,r}\dot\beta^i\beta^j\beta^p\beta^q\beta^r. \tag{2.21}$$

Tensors $\boldsymbol{V}$ are found by substituting (2.21) into (2.20) and collecting similar terms in β_i. The tensors $\boldsymbol{V}$ have no symmetry between the index i and other indexes (i corresponds to the summation by $\dot\beta^i$ and other indexes by β^k). The structure of (2.20) combined with (2.17) does not guarantee symmetry between indexes $jpqr$, which is why the commas between i, j, p, q and r are introduced.

The asymptotic technique gives

$$\left.\begin{aligned}
V^{2,n}_{a,b} &= \tfrac{1}{2}\Lambda^{(1)}_{nab} - (4E_nE_a)^{-1}\Pi^{(1)}_{na,b},\\
V^{3,n}_{a,b,c} &= (2E_n)^{-1}C_{nn}\Lambda^{(2)}_{nabc} - (4E_nE_a)^{-1}\Pi^{(2)}_{na,bc} - (2E_n)^{-1}V^{2,k}_{a,b}\Pi^{(1)}_{nk,c},\\
V^{4,n}_{a,b,c,d} &= \tfrac{1}{6}C_{nn}\Lambda^{(3)}_{nabcd} - (4E_nE_a)^{-1}\Pi^{(3)}_{na,bcd} - (2E_n)^{-1}V^{2,k}_{a,b}\Pi^{(2)}_{nk,cd}\\
&\quad -(2E_n)^{-1}V^{3,k}_{a,b,c}\Pi^{(1)}_{nk,d},\\
V^{5,n}_{a,b,c,d,f} &= \tfrac{1}{12}E_n^{-1}C^2_{nn}\Lambda^{(4)}_{nabcdf} - (4E_nE_a)^{-1}\Pi^{(4)}_{na,bcdf} - (2E_n)^{-1}V^{2,k}_{a,b}\Pi^{(3)}_{nk,cdf}\\
&\quad -(2E_n)^{-1}V^{3,k}_{a,b,c}\Pi^{(2)}_{nk,df} - (2E_n)^{-1}V^{4,k}_{a,b,c,d}\Pi^{(1)}_{nk,f}.
\end{aligned}\right\} \tag{2.22}$$

The time derivative of R^k is

$$\begin{aligned}
\dot R^k = (2E_k)^{-1}\ddot\beta_k + \ddot\beta^i(V^{2,k}_{i,j}\beta^j + V^{3,k}_{i,j,p}\beta^j\beta^p + V^{4,k}_{i,j,p,q}\beta^j\beta^p\beta^q + V^{5,k}_{i,j,p,q,r}\beta^j\beta^p\beta^q\beta^r)\\
+\dot\beta^i\dot\beta^j(V^{2,k}_{i,j} + 2\bar V^{3,k}_{i,jp}\beta^p + 3\bar V^{4,k}_{i,j,p,q}\beta^p\beta^q + 4\bar V^{5,k}_{i,j,p,q,r}\beta^p\beta^q\beta^r),
\end{aligned} \tag{2.23}$$

where

$$\left.\begin{aligned}
\bar V^{3,k}_{i,jp} &= \tfrac{1}{2}(V^{3,k}_{i,j,p} + V^{3,k}_{i,p,j}), \quad \bar V^{4,k}_{i,j,p,q} = \tfrac{1}{3}(V^{4,k}_{i,j,p,q} + V^{4,k}_{i,p,j,q} + V^{4,k}_{i,q,p,j}),\\
\bar V^{5,k}_{i,j,p,q,r} &= \tfrac{1}{4}(V^{5,k}_{i,j,p,q,r} + V^{5,k}_{i,p,j,q,r} + V^{5,k}_{i,q,p,j,r} + V^{5,k}_{i,r,p,q,j}).
\end{aligned}\right\} \tag{2.24}$$

The solution of (2.3) in the time-varying domain $Q(t)$ is required to calculate the integrals $l_\omega, l_{\omega t}$ and inertia tensor component J^1_{22}. This problem will be solved asymptotically in accordance with Narimanov's (1957) procedure. Since the angular velocity is assumed small, he proposed keeping only the polynomial terms depending on angular position, velocity and acceleration up to third order. The mixed polynomial terms like $\omega, \omega\beta_i, \omega^2\beta_i$ and $\omega\beta_i\beta_j$ are accounted for by Narimanov's theory. Since Narimanov assumed a third-order polynomial theory, these mixed terms agree with the general assumption. In accordance with polynomial expansion of A_n and A_{nk} some additional terms should be added for considering the fifth-order approximation. However, this is not possible due to mathematical limitations of the asymptotic procedure, discussed in some detail below.

https://doi.org/10.1017/S0022112000003311 Published online by Cambridge University Press

When starting Narimanov's asymptotic expansion, we get the following Neumann boundary problem in the mean fluid domain as a zero-order approximation:

$$\Delta\Omega_0 = 0 \quad \text{in } Q_0; \quad \frac{\partial\Omega_0}{\partial z} = -x \ (z = -h, z = 0); \quad \frac{\partial\Omega_0}{\partial x} = z \ (x = \pm\tfrac{1}{2}l). \tag{2.25}$$

It has the exact analytical solution in a Fourier series

$$\Omega_0 = xz - 2a_i f^i(x)F_i(z); \quad a_i = \frac{2l^2}{(i\pi)^3}X_i^{(0)}; \quad F_i(z) = \frac{\sinh(\varkappa_i(z + h/2))}{\cosh(\varkappa_i h/2)}, \tag{2.26}$$

where $X_i^{(0)}$ is the primary tensor of the $\boldsymbol{X}$-tensor set defined in Appendix A. Ω_0 is an infinite differentiable function in domain Q_0. But the series (2.26) allows only first and second derivatives on the mean free surface Σ_0 due to asymptotics of coefficients a_i for large i. The third derivative can be considered as a generalized function. Simple analysis shows that the second-order approximation needs the third derivatives of Ω_0, while the third-order approximation requires the fourth derivatives. The general theory of the Neumann boundary problem (see Marti 1986) shows that the third-order approximation problem is incorrect. The recursive problems up to the second-order approximation have a solution in the usual sense.

We pose an asymptotic solution of (2.3) as

$$\Omega = \Omega_0 + \Omega_1 + \Omega_2; \quad \Omega_k(x, z, t) = \chi_i^{(k)}(t)f^i(x)G_i(z); \quad G_i(z) = \frac{\cosh(\varkappa_i(z + h))}{\cosh(\varkappa_i h)}, \quad k = 1, 2, \tag{2.27}$$

where $\chi^{(k)}(t)$, $k = 1, 2$ are respectively linear and quadratic in $\beta^i(t)$ and index i implies summation from 1 to infinity.

The expression (2.27) satisfies the Laplace equation and all the boundary conditions except the Neumann boundary condition on the free surface. This condition is in a linear approximation

$$\left.\frac{\partial\Omega_1}{\partial z}\right|_{z=0} = -\left.\frac{\partial^2\Omega_0}{\partial z^2}\right|_{z=0} f + \left.\frac{\Omega_0}{\partial x}\right|_{z=0} f_x. \tag{2.28}$$

By substituting (2.27) into (2.28) we get

$$\Omega_1 = O_{\mu,k}^{(1)}\beta^k(t)f^\mu(x)G^\mu(z),$$

where

$$O_{\mu,k}^{(1)} = \frac{\varkappa^i a^i T^i(\varkappa_i \Lambda_{ki\mu}^{(1)} - \varkappa_k \Lambda_{ki,\mu}^{(-1)})}{2E_\mu}, \quad T^i = \tanh\left(\varkappa_i \frac{h}{2}\right). \tag{2.29}$$

Ω_2 satisfies the following boundary condition on Σ_0:

$$\left.\frac{\partial\Omega_2}{\partial z}\right|_{z=0} = -\frac{1}{2}\left.\frac{\partial^3\Omega_0}{\partial z^3}\right|_{z=0} f^2 + \left(\left.\frac{\partial^2\Omega_0}{\partial x\partial z}\right|_{z=0} - 1\right) f f_x + \left.\frac{\partial\Omega_1}{\partial x}\right|_{z=0} f_x - \left.\frac{\partial^2\Omega_1}{\partial z^2}\right|_{z=0} f. \tag{2.30}$$

This means that

$$\Omega_2 = O_{\mu,k,p}^{(2)}\beta^k(t)\beta^p(t)f^\mu(x)G^\mu(z),$$

where

$$O_{\mu,k,p}^{(2)} = \frac{X_i^{(0)}(l\varkappa^i)^{-1}(\varkappa_i \Lambda_{ikp\mu}^{(2)} - 2\varkappa_k \Lambda_{ik,p\mu}^{(-2)}) + \varkappa^i O_{i,k}^{(1)}(\varkappa_p \Lambda_{pi,\mu}^{(-1)} - \varkappa_i \Lambda_{pi\mu}^{(1)}))}{4E_q}. \tag{2.31}$$

https://doi.org/10.1017/S0022112000003311 Published online by Cambridge University Press

We can then write

$$\Omega = \Omega_0 + (O^{(1)}_{\mu,i}\beta^i(t) + O^{(2)}_{\mu,k,p}\beta^k(t)\beta^p(t))f^\mu(x)G^\mu(z). \tag{2.32}$$

When substituting (2.8) into (2.5), we find formally that the cubic approximation of Ω is needed to derive the terms with $\omega\beta_i\beta^j$ in the square brackets of (2.5). The following consequence of integral formulas show that (2.32) contains all the required terms. We can write

$$\begin{aligned}
&\left[\dot\omega\frac{\partial l_\omega}{\partial\beta_\mu} + \omega\frac{\partial l_{\omega t}}{\partial\beta_\mu} - \frac{\mathrm{d}}{\mathrm{d}t}\left(\omega\frac{\partial l_{\omega t}}{\partial\dot\beta_\mu}\right)\right] \Big/ \rho \\
&\quad = \dot\omega\frac{\partial}{\partial\beta_m}\int_Q \Omega\,\mathrm{d}Q - \dot\omega\frac{\partial}{\partial\dot\beta_\mu}\int_Q\frac{\partial\Omega}{\partial t}\,\mathrm{d}Q + \omega\frac{\partial}{\partial\beta_\mu}\int_Q\frac{\partial\Omega}{\partial t}\,\mathrm{d}Q - \omega\frac{\mathrm{d}}{\mathrm{d}t}\frac{\partial}{\partial\dot\beta_\mu}\int_Q\frac{\partial\Omega}{\partial t}\,\mathrm{d}Q \\
&\quad = \dot\omega\left[\int_{-l/2}^{l/2}\Omega\Big|_{z=f} f_\mu\,\mathrm{d}x + \int_Q\frac{\partial\Omega}{\partial\beta_\mu}\,\mathrm{d}Q - \int_Q\frac{\partial^2\Omega}{\partial\dot\beta_m\partial t}\,\mathrm{d}Q\right] \\
&\qquad + \omega\left[\int_{-l/2}^{l/2}\frac{\partial\Omega}{\partial t}\Big|_{z=f} f_\mu\,\mathrm{d}x + \int_Q\frac{\partial^2\Omega}{\partial\beta_\mu\partial t}\,\mathrm{d}Q - \frac{\mathrm{d}}{\mathrm{d}t}\int_Q\frac{\partial\Omega}{\partial\beta_m}\,\mathrm{d}Q\right] \\
&\quad = \dot\omega\int_{-l/2}^{l/2}\Omega\Big|_{z=f} f_\mu\,\mathrm{d}x + \omega\int_{-l/2}^{l/2}\frac{\partial\Omega}{\partial t}\Big|_{z=f} f_\mu\,\mathrm{d}x - \omega\int_{-l/2}^{l/2}\frac{\partial\Omega}{\partial\beta_\mu}\Big|_{z=f} f_t\,\mathrm{d}x,
\end{aligned} \tag{2.33}$$

where we used that Ω_0 does not depend on β_μ and the following differential relations:

$$\frac{\partial\Omega}{\partial\beta_\mu} = \frac{\partial^2\Omega}{\partial\dot\beta_\mu\partial t}, \quad \frac{\partial^2\Omega}{\partial\beta_\mu\partial t} = \frac{\partial^2\Omega}{\partial t\partial\beta_\mu}.$$

The last three integrals of (2.33) can be expanded in power series. This gives

$$\rho\frac{l}{2}[\dot\omega(L^{(0)}_\mu + \beta^i L^{(1)}_{i,\mu} + \beta^k\beta^p L^{(2)}_{k,p,\mu}) + \omega(\dot\beta^i L^{(3)}_{i,\mu} + \dot\beta^k\beta^p L^{(4)}_{k,p,\mu})], \tag{2.34}$$

where

$$L^{(0)}_\mu = -4X^{(0)}_\mu l^{-1}(\varkappa_\mu)^{-3}T_\mu, \quad L^{(1)}_{i,\mu} = O^{(1)}_{\mu,i} - l\pi^{-2}X^{(1)}_{i\mu}, \tag{2.35}$$

$$L^{(2)}_{k,p,\mu} = O^{(2)}_{\mu,k,p} + E^m O^{(1)}_{m,k}\Lambda^{(1)}_{mp\mu} - T^m X^{(0)}_m(2\pi m)^{-1}\Lambda^{(2)}_{mkp\mu}, \tag{2.36}$$

$$L^{(3)}_{i,\mu} = O^{(1)}_{\mu,i} - O^{(1)}_{i,\mu}; \quad L^{(4)}_{k,p,\mu} = 2(\bar O^{(2)}_{\mu,kp} - \bar O^{(2)}_{k,\mu p}) + E^m(O^{(1)}_{m,k}\Lambda^{(1)}_{mp\mu} - O^{(1)}_{m,\mu}\Lambda^{(1)}_{mkp}). \tag{2.37}$$

Tensors $\boldsymbol{X}$ are defined in Appendix A.

The scalar function J^1_{22} (the component of the inertia tensor introduced by Faltinsen *et al.* 2000) should be expanded in β^i up to quadratic terms, i.e.

$$J^1_{22} = \rho l(J^{(0)} + \beta^k J^{(1)}_k + \beta^k\beta^p J^{(2)}_{k,p}). \tag{2.38}$$

Direct asymptotic expansion gives

$$J^{(0)} = \frac{h}{3}(h^2 - 0.25l^2) - \sum_{i=1}^{\infty}\frac{4}{l^2\varkappa_i^5}(X^{(0)}_i)^2[h\varkappa_i - 4T_i], \tag{2.39}$$

$$J^{(1)}_k = (\varkappa_k)^{-2}X^{(-0)}_k - \sum_{i=1}^{\infty}O^{(1)}_{i,k}\frac{4}{l\varkappa_i}X^{(0)}_i T_i E_i, \tag{2.40}$$

https://doi.org/10.1017/S0022112000003311 Published online by Cambridge University Press

$$J^{(2)}_{k,p} = \sum_{i=1}^{\infty} \left(\frac{lT_i}{\pi^3 i^2} X^{(0)}_i [iX^{(2)}_{ikp} - Y^{(2)}_{i,kp}] - O^{(1)}_{i,k} E_i l \pi^{-2} X^{(1)}_{ip} - 4l^{-1} O^{(2)}_{i,k,p} \varkappa_i^{-3} X^{(0)}_i T_i E_i \right), \tag{2.41}$$

where $\boldsymbol{Y}$-tensors are calculated in Appendix A.

The inertia term in (2.5) can be expressed as

$$-\omega^2 \frac{1}{2} \frac{\partial J^1_{22}}{\partial \beta_\mu} = -\rho\omega^2 \frac{l}{2} (J^{(1)}_\mu + 2\bar{J}^{(2)}_{\mu p} \beta^p), \quad \bar{J}^{(2)}_{\mu p} = \tfrac{1}{2}(J^{(2)}_{\mu,p} + J^{(2)}_{p,\mu}). \tag{2.42}$$

Now we can substitute (2.15), (2.19), (2.21), (2.24), (2.34), (2.38) and (2.42) into (2.5). We get, correct to fifth order in β_i and third order for terms containing angular position and angular velocity, that

$$\begin{aligned}
&\ddot{\beta}^a (\delta_{a\mu} + d^{1,\mu}_{a,b}\beta^b + d^{2,\mu}_{a,b,c}\beta^b\beta^c + d^{3,\mu}_{a,b,c,d}\beta^b\beta^c\beta^d + d^{4,\mu}_{a,b,c,d,f}\beta^b\beta^c\beta^d\beta^f) \\
&+\dot{\beta}^a\dot{\beta}^b (t^{0,\mu}_{a,b} + t^{1,\mu}_{a,b,c}\beta^c + t^{2,\mu}_{a,b,c,d}\beta^c\beta^d + t^{3,\mu}_{a,b,c,d,f}\beta^c\beta^d\beta^f) + \sigma^2_\mu \beta_\mu \\
&+P_\mu(\dot{v}_{0x} + \omega v_{0z} - g\sin\psi) + Q_\mu\beta_\mu(\dot{v}_{0z} - \omega v_{0x} - g(1 - cos\psi)) - \omega^2 Q_\mu (J^{(1)}_\mu + \beta^p 2\bar{J}^{(2)}_{\mu p}) \\
&+\dot{\omega} Q_\mu (L^{(0)}_\mu + \beta^i L^{(1)}_{i,\mu} + \beta^k\beta^p L^{(2)}_{k,p,\mu}) + \omega Q_\mu (\dot{\beta}^i L^{(3)}_{i,\mu} + \dot{\beta}^k\beta^p L^{(4)}_{k,p,\mu}) = 0, \quad \mu \geqslant 1,
\end{aligned} \tag{2.43}$$

where

$$\sigma^2_\mu = 2E_\mu g, \quad \mu \geqslant 1; \quad P_{2i-1} = -\frac{8E_{2i-1}l}{\pi^2(2i-1)^2}, \quad P_{2i} = 0, \quad i \geqslant 1, \quad Q_\mu = 2E_\mu. \tag{2.44}$$

Here σ_μ is the natural frequency of the μth mode, ψ is the angular position and g is the acceleration due to gravity.

Further

$$d^{1,\mu}_{a,b} = 2E_\mu(\tfrac{1}{2}\Lambda^{(1)}_{ab\mu} + V^{2,\mu}_{a,b}), \tag{2.45}$$

$$d^{2,\mu}_{a,b,c} = 2E_\mu((2E_a)^{-1} C_{aa} \Lambda^{(2)}_{abc\mu} + E_n \Lambda^{(1)}_{nc\mu} V^{2,n}_{a,b} + V^{3,\mu}_{a,b,c}), \tag{2.46}$$

$$d^{3,\mu}_{a,b,c,d} = 2E_\mu(\tfrac{1}{6} C_{aa} \Lambda^{(3)}_{abcd\mu} + C_{nn} \Lambda^{(2)}_{ncd\mu} V^{2,n}_{a,b} + E_n \Lambda^{(1)}_{nd\mu} V^{3,n}_{a,b,c} + V^{4,\mu}_{a,b,c,d}), \tag{2.47}$$

$$\begin{aligned}
d^{4,\mu}_{a,b,c,d,f} = 2E_\mu(&\tfrac{1}{12} C^2_{aa} E^{-1}_a \Lambda^{(4)}_{abcdf\mu} + \tfrac{1}{3} C_{nn} E_n \Lambda^{(3)}_{ncdf\mu} V^{2,n}_{a,b} + C_{nn} \Lambda^{(2)}_{ndf\mu} V^{3,n}_{a,b,c} \\
&+E_n \Lambda^{(1)}_{nf\mu} V^{4,n}_{a,b,c,d} + V^{5,\mu}_{a,b,c,d,f}),
\end{aligned} \tag{2.48}$$

$$t^{0,\mu}_{a,b} = 2E_\mu(V^{2,\mu}_{a,b} + (8E_aE_b)^{-1} \Pi^{(1)}_{ab,\mu}), \tag{2.49}$$

$$t^{1,\mu}_{a,b,c} = 2E_\mu(2\bar{V}^{3,\mu}_{a,b,c} + V^{2,n}_{a,b} E_n \Lambda^{(1)}_{nc\mu} + (4E_aE_b)^{-1} \Pi^{(2)}_{ab,\mu c} + (2E_a)^{-1} V^{2,n}_{b,c} \Pi^{(1)}_{an,\mu}), \tag{2.50}$$

$$\begin{aligned}
t^{2,\mu}_{a,b,c,d} = 2E_\mu(&3\bar{V}^{4,\mu}_{a,b,c,d} + 2\bar{V}^{3,n}_{a,b,c} E_n \Lambda^{(1)}_{nd\mu} + V^{2,n}_{a,b} C_{nn} \Lambda^{(2)}_{ncd\mu} + \tfrac{3}{8} \Pi^{(3)}_{ab,cd\mu} (E_aE_b)^{-1} \\
&+\Pi^{(2)}_{bn,c\mu} E^{-1}_b V^{2,n}_{a,d} + (2E_b)^{-1} V^{3,n}_{a,c,d} \Pi^{(1)}_{bn,\mu} + \tfrac{1}{2} \Pi^{(1)}_{nk,\mu} V^{2,k}_{a,c} V^{2,n}_{b,d}),
\end{aligned} \tag{2.51}$$

$$\begin{aligned}
t^{3,\mu}_{a,b,c,d,f} = 2E_\mu(&4\bar{V}^{5,\mu}_{a,b,c,d,f} + 3\bar{V}^{4,n}_{a,b,c,d} E_n \Lambda^{(1)}_{nf\mu} + 2\bar{V}^{3,n}_{a,b,c} C_{nn} \Lambda^{(2)}_{ndf\mu} + \tfrac{1}{3} V^{2,n}_{a,b} C_{nn} E_n \Lambda^{(3)}_{ncdf\mu} \\
&+\tfrac{1}{2} \Pi^{(4)}_{ab,\mu cdf} (E_aE_b)^{-1} + \tfrac{3}{2} \Pi^{(3)}_{na,cd\mu} E^{-1}_a V^{2,n}_{b,f} + \Pi^{(2)}_{na,f\mu} E^{-1}_a V^{3,n}_{b,c,d} \\
&+\Pi^{(2)}_{nk,f\mu} V^{2,k}_{a,c} V^{2,n}_{b,d} + \Pi^{(1)}_{an,\mu} (2E_a)^{-1} V^{4,n}_{b,c,d,f} + \Pi^{(1)}_{nk,\mu} V^{3,n}_{a,c,d} V^{2,k}_{b,f}).
\end{aligned} \tag{2.52}$$

https://doi.org/10.1017/S0022112000003311 Published online by Cambridge University Press

2.3. *Hydrodynamic force and moment on the tank*

The formulas below use coordinates (x_C, z_C) of the fluid centre of mass in a tank with infinite roof height, i.e.

$$x_C = -\frac{l}{\pi^2 h}\sum_{i=1}^{\infty}\beta_i(t)\frac{1}{i^2}(1+(-1)^{i+1}), \quad z_C = -\frac{h}{2}+\frac{1}{4h}\sum_{i=1}^{\infty}\beta_i^2(t). \tag{2.53}$$

Our force calculations are based on the formula derived by Lukovsky (1990):

$$\boldsymbol{F} = m\boldsymbol{g} - m[\dot{\boldsymbol{v}}_0 + \boldsymbol{\omega}\times\boldsymbol{v}_0 + \boldsymbol{\omega}\times(\boldsymbol{\omega}\times\boldsymbol{r}_C) + \dot{\boldsymbol{\omega}}\times\boldsymbol{r}_C + 2\boldsymbol{\omega}\times\dot{\boldsymbol{r}}_C + \ddot{\boldsymbol{r}}_C]. \tag{2.54}$$

Here m is the fluid mass, $\boldsymbol{r}_C$ is the radius-vector of the centre of mass in the moving coordinate system and $m\boldsymbol{g}$ is the fluid weight. The terms in square brackets are: $\dot{\boldsymbol{v}}_0$ the acceleration of the origin O, $\boldsymbol{\omega}\times\boldsymbol{v}_0$ the tangential acceleration, $\boldsymbol{\omega}\times(\boldsymbol{\omega}\times\boldsymbol{r}_C)$ the centripetal acceleration, $2\boldsymbol{\omega}\times\dot{\boldsymbol{r}}_C$ Coriolis acceleration, $\ddot{\boldsymbol{r}}_C$ the relative acceleration.

The force $(F_x, 0, F_z)$ in two-dimensional flow can then be written as

$$F_x = mg_1 - m(\dot{v}_{0x} + \omega v_{0z} - \omega^2 x_C + \dot{\omega} z_C + 2\omega\dot{z}_C + \ddot{x}_C), \tag{2.55}$$

$$F_z = mg_3 - m(\dot{v}_{0z} - \omega v_{0x} - \omega^2 z_C - \dot{\omega} x_C - 2\omega\dot{x}_C + \ddot{z}_C), \tag{2.56}$$

where the coordinates x_C, z_C are defined by (2.53) and the projections g_1, g_3 of the gravity vector on the Oxz axes are

$$g_1 = g\sin\psi, \quad g_3 = -g\cos\psi. \tag{2.57}$$

The hydrodynamic moment relative to axis Oy can also be calculated by the formula derived by Lukovsky (1990)

$$\boldsymbol{M}_0 = m\boldsymbol{r}_C\times(\boldsymbol{g}-\boldsymbol{\omega}\times\boldsymbol{v}_0-\dot{\boldsymbol{v}}_0)-\boldsymbol{J}^1\cdot\dot{\boldsymbol{\omega}}-\dot{\boldsymbol{J}}^1\cdot\boldsymbol{\omega}-\boldsymbol{\omega}\times(\boldsymbol{J}^1\cdot\boldsymbol{\omega})-\ddot{\boldsymbol{l}}_\omega+\dot{\boldsymbol{l}}_{\omega t}-\boldsymbol{\omega}\times(\dot{\boldsymbol{l}}_\omega-\boldsymbol{l}_{\omega t}), \tag{2.58}$$

where $\boldsymbol{J}^1$ is the inertia tensor, the scalar components of which were defined by Faltinsen *et al.* (2000). For two-dimensional flows we need only one scalar component J^1_{22} given by (2.8).

To calculate the hydrodynamic moment relative to the other axis through point P we can use

$$\boldsymbol{M}_P = \boldsymbol{r}_{PO}\times\boldsymbol{F} + \boldsymbol{M}_0, \tag{2.59}$$

where the hydrodynamic force is given by (2.54).

The formula (2.58) does not have a simple structure because of the term $\ddot{l}_\omega - \dot{l}_{\omega t}$. By using the derivations above we find

$$\dot{l}_\omega - l_{\omega t} = \rho\frac{l}{2}(\dot{\beta}^m L^{(0)}_m + \dot{\beta}^m\beta^p L^{(1)}_{p,m} + \dot{\beta}^m\beta^n\beta^p L^{(2)}_{k,p,m}), \tag{2.60}$$

where $L^{(0)}, L^{(1)}, L^{(2)}$ are calculated by (2.35)–(2.36). The pitch moment about O in two-dimensional flow, $\boldsymbol{M}_0 = (0, M, 0)$, can be written as

$$\begin{aligned} M = {} & m(x_C(-g_3 - v_{0x}\omega + \dot{v}_{0z}) - z_C(-g_1 + \omega v_{0z} + \dot{v}_{0x})) - \rho l\dot{\omega}(J^{(0)} + \beta^k J^{(1)}_k + \beta^k\beta^p J^{(2)}_{k,p}) \\ & -\rho l(\dot{\beta}^k J^{(1)}_k + 2\bar{J}^{(2)}_{kp}\dot{\beta}^k\beta^p)\omega - \rho\frac{l}{2}(\ddot{\beta}^m L^{(0)}_m + \ddot{\beta}^m\beta^p L^{(1)}_{p,m} + \ddot{\beta}^m\beta^k\beta^p L^{(2)}_{k,p,m} \\ & + L^{(1)}_{p,m}\dot{\beta}^m\dot{\beta}^p + 2\bar{L}^{(2)}_{kp,m}\dot{\beta}^m\dot{\beta}^k\beta^p), \end{aligned} \tag{2.61}$$

where $J^{(0)}, J^{(1)}, J^{(2)}$ are given by (2.39)–(2.41) and

$$\bar{L}^{(2)}_{kp} = \tfrac{1}{2}(L^{(2)}_{k,p} + L^{(2)}_{p,k}).$$

https://doi.org/10.1017/S0022112000003311 Published online by Cambridge University Press

3. Surge- and pitch-excited resonant sloshing

3.1. *Modal system for resonant sloshing*

For resonant sloshing with small forced excitation amplitude the magnitudes of ω, ψ, and $\dot{v}_{0x}$ are formally associated with the small parameter ϵ. Terms $o(\epsilon)$ will be omitted. Modal system (2.43) then takes the form

$$\ddot{\beta}_\mu + \sum_{a,b=1}^{\infty} d^{1,\mu}_{a,b}\ddot{\beta}^a\beta^b + \sum_{a,b,c=1}^{\infty} d^{2,\mu}_{a,b,c}\ddot{\beta}^a\beta^b\beta^c + \sum_{a,b,c,d=1}^{\infty} d^{3,\mu}_{a,b,c,d}\ddot{\beta}^a\beta^b\beta^c\beta^d$$

$$+ \sum_{a,b,c,d,f=1}^{\infty} d^{4,\mu}_{a,b,c,d,f}\ddot{\beta}^a\beta^b\beta^c\beta^d\beta^f + \sum_{a,b=1}^{\infty} t^{0,\mu}_{a,b}\dot{\beta}^a\dot{\beta}^b + \sum_{a,b,c=1}^{\infty} t^{1,\mu}_{a,b,c}\dot{\beta}^a\dot{\beta}^b\beta^c$$

$$+ \sum_{a,b,c,d=1}^{\infty} t^{2,\mu}_{a,b,c,d}\dot{\beta}^a\dot{\beta}^b\beta^c\beta^d + \sum_{a,b,c,d,f=1}^{\infty} t^{3,\mu}_{a,b,c,d,f}\dot{\beta}^a\dot{\beta}^b\beta^c\beta^d\beta^f$$

$$+ \sigma^2_\mu\beta_\mu + P_\mu(\dot{v}_{0x} - g\psi) + \dot{\omega}Q_\mu L^{(0)}_\mu = 0, \quad \mu \geqslant 1. \tag{3.1}$$

The terms associated with J^1_{22} have higher order in this approximation. However, inertia terms are present in formulas for lateral force and pitch moment. These formulas are, correct to $O(\epsilon)$,

$$F_x = mg\psi - m(\dot{v}_{0x} + \dot{\omega}z^{(0)}_C + \ddot{x}_C); \quad F_z = -mg - m(\dot{v}_{0z} + \ddot{z}_C), \tag{3.2}$$

$$M = m(x_C g - z^{(0)}_C(\dot{v}_{0x} - g\psi)) - \rho l\dot{\omega}J^{(0)}$$

$$-\rho\frac{l}{2}(\ddot{\beta}^m L^{(0)}_m + \ddot{\beta}^m\beta^p L^{(1)}_{p,m} + \ddot{\beta}^m\beta^k\beta^p L^{(2)}_{k,p,m} + L^{(1)}_{p,m}\dot{\beta}^m\dot{\beta}^p + 2\bar{L}^{(2)}_{kp,m}\dot{\beta}^m\dot{\beta}^k\beta^p), \tag{3.3}$$

where $z^{(0)}_C = -h/2$ is the vertical coordinate of the centre of gravity of 'frozen' fluid mass.

Modal system (3.1) does not set up a preference relation for a single dominant β_i. All the modes have been formally incorporated with the same order. The system has a simple polynomial structure and many coefficients d and t of this system are zero. However, a strategy (truncating procedure) is required to reduce the system to finite-dimensional form prior to numerical simulations. The direct implementation of this uniformly structured system is questionable if the truncating procedure is based on simple limitation of the sum by a finite number N (see Appendix B). The number of non-zero coefficients can be large even for a small number of equations. The system (B 1) has for instance more than 1000 non-zero coefficients for $N = 5$. Another difficulty is due to high harmonics in primary modes caused by the response of high modes. So, for example, a term proportional to $\ddot{\beta}_1\beta^4_5$ can appear in the first equation of (3.1); β_1 and β_5 have respectively σ and 5σ as main harmonics. This gives an oscillatory term with frequency 21σ in β_1 and leads to a very stiff nonlinear system of ordinary differential equations. The numerical time integration is then inefficient and easily becomes unstable. It was only possible to calculate a few seconds of real time with our numerical integrator. This unrealistically stiff system is caused by neglecting a series of physical phenomena and real asymptotic inter-modal relations. Surface tension and damping can be important in avoiding high harmonics. Since energy dissipation is not present in our theoretical model, additional coefficients associated with damping of different modes have to be incorporated. The effect of damping

https://doi.org/10.1017/S0022112000003311 Published online by Cambridge University Press

due to viscosity and surface tension should be further investigated. The studies by Keulegan (1959), Miles (1990), Cocciaro *et al.* (1991) and Miles & Henderson (1998) are useful in this context. In addition, when using the polynomial approximation we implicitly assume both smallness and relations between the β_i of polynomial type. High-order or transcendental inter-modal interactions are neglected even if they are important. This means that our fifth-order system cannot be considered as an approximate modal system but only as the base for various asymptotic theories. Such asymptotic theories assume a finite number of dominating modes and need a detuning procedure by introducing appropriate relations between the β_i.

3.2. *Detuning procedure for a single dominant model*

One way to tune the system is to give the summations of (3.1) an analytical condition coupling the indexes of summations. In particular, if the sum of indexes does not exceed 3 (order of the theory), we arrive at the modal system by Faltinsen *et al.* (2000) describing the sloshing with dominating lowest primary mode

$$\left.\begin{aligned} &\ddot{\beta}_1(1 + D1^1(1,2)\beta_2 + D2^1(1,1,1)\beta_1^2) + D1^1(2,1)\ddot{\beta}_2\beta_1 + T0^1(1,1,1)\dot{\beta}_1\dot{\beta}_1\beta_1 \\ &\quad + T0^1(2,1)\dot{\beta}_1\dot{\beta}_2 + \sigma_1^2\beta_1 + P_1(\dot{v}_{0x} - g\psi) + \dot{\omega}Q_1L_1^{(0)} = 0, \\ &\quad D1^2(1,1)\ddot{\beta}_1\beta_1 + \ddot{\beta}_2 + T0^2(1,1)\dot{\beta}_1\dot{\beta}_1 + \sigma_2^2\beta_2 = 0. \end{aligned}\right\} \tag{3.4}$$

The coefficients of (3.4) (see Appendix B) coincide with the ones derived by Faltinsen *et al.* (2000). This is an explicit verification of these theories. A third equation, which contains β_3 linearly and β_1, β_2 nonlinearly, can be added to the system (3.4). This means that the third mode is considered as driven by primary and secondary modal functions. The modal system of the fifth-order theory by Waterhouse (1994) can be derived in a similar way from (3.1).

3.3. *Detuning procedure for a secondary resonance*

In a rectangular tank excited by surge and pitch we can predict direct resonance for odd modes. This is due to $P_{2i} = Q_{2i} = 0$ in the modal equation. Secondary resonance is explained by the nonlinear terms and can occur for any mode. The single dominant model obtained by Faltinsen *et al.* (2000) gives a prediction of secondary resonance for the secondary mode in steady-state motion. When the excitation amplitude is sufficiently small, this happens for an excitation period domain in the neighbourhood of

$$\frac{T}{T1} = \frac{\sigma_1}{\sigma} \to \sqrt{\frac{2\tanh(\pi h/l)}{\tanh(2\pi h/l)}} = i(2, h/l). \tag{3.5}$$

Here $T1$ is the highest natural period of fluid oscillations. Similarly, if we expect the harmonic $m\sigma$ to be dominating in each mth mode we can derive from modal system (3.1) that

$$\frac{T}{T1} = \frac{\sigma_1}{\sigma} \to i(m, h/l) = \sqrt{\frac{m\tanh(\pi h/l)}{\tanh(m\pi h/l)}}. \tag{3.6}$$

Note that the position of secondary resonance does not depend on the excitation amplitude and wave amplitude response of the primary mode in this approximation. The theory does not give the value of the effective domain for primary and secondary resonance, which grows with excitation amplitude. For a sufficiently small resonance response the effective domains do not overlap each other. But overlapping can happen for sufficiently large wave amplitude. In addition, the effective domains can undergo

https://doi.org/10.1017/S0022112000003311 Published online by Cambridge University Press

a downshift or upshift. This also leads to overlapping of these domains. Two or more modes having the same order are then involved in resonant sloshing.

Our system has a general multidimensional structure, which can be adapted to a multimodal resonant excitation. A preliminary analysis is required to start the simulation of steady-state solutions. The analysis is connected with an *a priori* prediction of inter-modal resonances. In simplified form it can be treated with the following adaptive procedure. We consider a series of natural frequencies $\sigma_1, \sigma_2, \sigma_3, \ldots$ and a set of possible frequencies $\sigma, 2\sigma, 3\sigma, \ldots$ caused by the main excitation frequency σ. If σ is close to one of the natural frequencies of the odd modes and far from the other modes, this mode is a primary excited one. In order to add the most dangerous secondary resonance we should find the mode (even or odd) for which the natural frequency is close to 2σ.

Let us assume as an example that these two modes correspond to β_1 and β_2. The two first nonlinear equations of the general system give a kernel of this interaction. Any other mode β_m can be considered as having lower order or driven (they are linear in β_m and nonlinear in dominating modes). The secondary resonance implies $\beta_2 \sim \beta_1$. This means that additional nonlinear terms in β_1 and β_2 should be included. Two of the equations take then the following form:

$$\left.\begin{aligned}
&\ddot{\beta}_1(1 + D1^1(1,2)\beta_2 + D2^1(1,1,1)\beta_1^2 + D2^1(1,2,2)\beta_2^2) + \ddot{\beta}_2(D1^1(2,1)\beta_1 \\
&\quad + D2^1(2,2,1)\beta_2\beta_1) + T0^1(1,1,1)\dot{\beta}_1\dot{\beta}_1\beta_1 + T1^1(2,2,1)\dot{\beta}_2\dot{\beta}_2\beta_1 \\
&\quad + \dot{\beta}_1\dot{\beta}_2(T0^1(2,1) + T1^1(2,1,2)\beta_2) + \sigma_1^2\beta_1 + P_1(\dot{v}_{0x} - g\psi) + \dot{\omega}Q_1L_1^{(0)} = 0, \\
&\ddot{\beta}_1(D1^2(1,1)\beta_1 + D2^2(1,2,1)\beta_1\beta_2) + \ddot{\beta}_2(1 + D2^2(2,1,1)\beta_1^2 + D2^2(2,2,2)\beta_2^2) \\
&\quad + \dot{\beta}_1\dot{\beta}_1(T0^2(1,1) + T1^2(1,1,2)) + T1^2(2,2,2)\dot{\beta}_2\dot{\beta}_2\beta_2 \\
&\quad + T1^2(2,1,1)\dot{\beta}_1\dot{\beta}_2\beta_1 + \sigma_2^2\beta_2 = 0.
\end{aligned}\right\} \tag{3.7}$$

This system is of third polynomial order in β_1 and β_2. It contains all the necessary terms of Faltinsen–Moiseyev theory and a theory considering $\beta_1 \sim \beta_2 = O(\epsilon^{1/2})$. In addition, the third-order terms similar to β_2^3, $\beta_2^2\beta_1$ are included to describe a 'switch' between these asymptotics during transients when $\beta_1 \sim \beta_2 = O(\epsilon^{1/3})$ in the framework of a third-order theory. The responses of third and fourth modes are not included in the equations presented. They can be considered as driven and follow from (3.1) when no corresponding high-mode secondary resonance occurs. Four equations for $\beta_3, \beta_4, \beta_5$ and β_6 are nonlinear in β_1 and β_2 and linear in $\beta_3, \beta_4, \beta_5$ and β_6 respectively.

When the three modes β_1, β_2 and β_3 have the same order, the corresponding nonlinear system of differential equations can be derived in a similar way. It couples three modal functions up to terms of third order. A similar procedure can also be followed for the primary excited non-lowest natural mode.

Although we derived (3.7) to describe steady-state solutions, it can be used for simulation of beating waves. These waves appear at the initial phase due to nonlinear interaction between natural and forced solutions.

3.4. *Adaptive detuning procedure*

Modal functions in the general case can be associated with an order $\beta_i = O(\epsilon^{p_i/K})$, where K is the order of the theory and $p_i \leqslant K$. The analytical conditions in summations should couple p_i instead of indexes i. In order to keep only terms of $O(\epsilon)$ in (3.1) we use the condition $\sum p_i \leqslant K$. For example, $\sum_{a,b,c,d=1}^{\infty}$ should be accompanied by condition $p_a + p_b + p_c + p_d \leqslant K$. These conditions allow us to avoid analytical

https://doi.org/10.1017/S0022112000003311 Published online by Cambridge University Press

manipulations to derive particular cases of the uniformly valid system detuned for different sets of p_i.

4. Comparison between theory and experiments

Some series of experiments on resonant surge- and pitch-excited nonlinear sloshing are used for validation. Olsen & Johnsen (1975) and Olsen (1970, personal communication) presented results for a tank with rectangular cross-sectional shape (see figure 2*a*). Abramson *et al.* (1974) and Mikelis *et al.* (1984) (see also Delft University Report 1983) used in their experimental studies the prismatic tanks shown in respectively figures 2(*b*) and 2(*d*). These experimental series give the measured wave amplitude near the wall, longitudinal force and pitch moment for large-amplitude steady-state sloshing. We cannot therefore validate the adaptive procedure for large-amplitude sloshing during the initial phase by using these experimental data. However, the experiments by Faltinsen *et al.* (2000) in a surge-excited rectangular tank (see figure 2*c*) provide a recording of the wave amplitude when violent sloshing starts from an initially unperturbed planar surface. They will be used to validate our adaptive method for a case with small fluid depth where the modal theory by Faltinsen *et al.* (2000) failed.

Although our theory assumes a rectangular tank, it will be applied to prismatic tanks. The error in doing so will be assessed by examining the eigenvalues. A rough estimate of eigenvalues $\tilde{\sigma}_i^2$ relative to eigenvalues σ_i^2 of a virtual rectangular tank with the same fluid depth and maximum tank breadth as a prismatic tank can be made by using the Rayleigh–Kelvin variational formula

$$\tilde{\sigma}_i^2 = g\frac{\displaystyle\int_{\tilde{Q}_0}(\nabla\varphi_i)^2\,\mathrm{d}Q}{\displaystyle\int_{\Sigma_0}\varphi_i\,\mathrm{d}S}$$

(see Feschenko *et al.* 1969). Here $\tilde{Q}_0$ is the mean volume of fluid in the prismatic tank and the φ_i are natural modes in the rectangular tank. The result is

$$\frac{\sigma_i^2-\tilde{\sigma}_i^2}{\sigma_i^2} = 2\frac{\pi\mathrm{i}}{\tanh(\mathrm{i}\pi h/l)}\left(\frac{\sin^2(\mathrm{i}\pi\delta_1/l)+\sinh^2(\mathrm{i}\pi\delta_2)}{\cosh^2(\mathrm{i}\pi h/l)}\right)\frac{\delta_1\delta_2}{l^2},$$

where δ_1 and δ_2 are respectively the breadth and height of the corners (see figure 3). If this is applied to the lowest mode of the tank in figure 2(*b*) when $h/l = 0.4$, it gives $(\sigma_1^2-\tilde{\sigma}_1^2)/\sigma_1^2 = 0.0081\ldots$. When applied to the tank in figure 2(*d*) with $h/l = 0.246$, it gives $(\sigma_1^2-\tilde{\sigma}_1^2)/\sigma_1^2 = 0.03$. The error decreases with increasing mode number. The reason is simply that the higher modes are affected to a much less extent by the tank bottom.

We use as a basis for our studies the theoretical prediction of steady-state solutions given by the single dominant theory by Faltinsen *et al.* (2000). The theory gives the wave amplitude response A of the lowest primary mode versus excitation period coupled by a cubic secular equation $((T/T1)^2-1)(A/l)+m_1(h/l, T/T1)(A/l)^3 = P_1H$, where P_1H is a dimensionless excitation amplitude. This secular equation was derived by Faltinsen (1974) through the Moiseyev procedure and by Faltinsen *et al.* (2000) in the context of modal approximation (3.4). (We should note that in the modal approximation the coefficient m_1 is a function of excitation period unlike the secular equation derived by a Moiseyev-like asymptotic procedure. This is extensively

https://doi.org/10.1017/S0022112000003311 Published online by Cambridge University Press

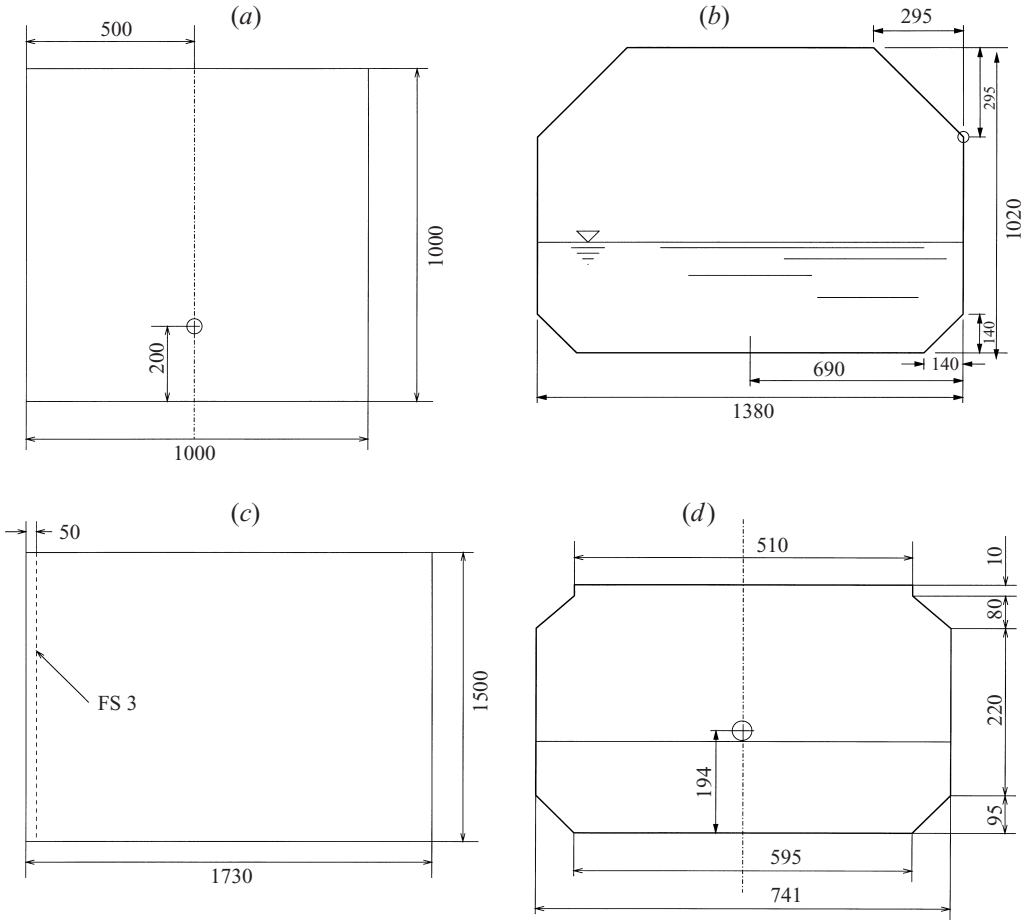


FIGURE 2. (*a*) Rectangular tank used by Olsen & Johnsen (1975) and Olsen (1970, personal communication). (*b*) Prismatic tank used by Abramson *et al.* (1974). (*c*) Rectangular tank used by Faltinsen *et al.* (2000). (*d*) Prismatic tank used by Mikelis *et al.* (1984). All numbers in mm. $\oplus$ means the position of the rotation axis.

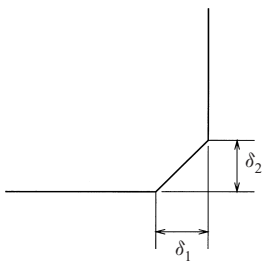


FIGURE 3. Dimensions of the lower corner in a prismatic tank.

discussed by Faltinsen *et al.* (2000). The equations coincide when $T = T1$ in m_1.) This and many other papers using the single dominant asymptotic approach (see, for example, Ockendon & Ockendon 1973; Shemer 1990 and Tsai *et al.* 1990) report the existence of at least one stable steady-state solution as $T \to T1$, introduce two types of branches in the $(T/T1, A/l)$-plane showing these solutions and discuss the

https://doi.org/10.1017/S0022112000003311 Published online by Cambridge University Press

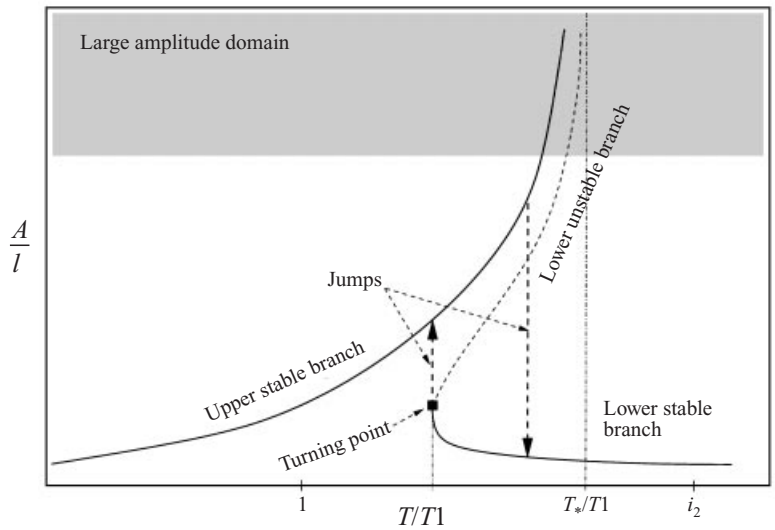


FIGURE 4. The 'soft spring'-type amplitude response in accordance with the modal theory by Faltinsen *et al.* (2000). The fluid depth exceeds the critical value $h/l = 0.3374\ldots$.

hysteresis in the steady-state fluid response, the dependence of branches on excitation amplitude, the downshift (upshift) of the maximum amplitude response and so on.

Figure 4 shows schematically these theoretical predictions in accordance with theoretical results by Faltinsen *et al.* (2000) for a 'soft spring'-type response (the classification 'soft spring' ('hard spring') solutions is adopted from characteristics of the Duffing equation). The first (upper) branch in figure 4 implies stable solutions. The second (lower) branch displays stable and unstable steady-state solutions with a turning point between them. The set of turning points for different excitation amplitudes H can be found from the equation $((T/T1)^2 - 1) + 3m_1(h/l, T/T1)(A/l)^2 = 0$. The ordinate $T/T1$ of the turning point defines a jump from the lower to upper branch. Another jump from the upper to lower branch occurs as A/l increases along the upper branch. It occurs for sufficiently large sloshing amplitudes (breakdown is caused by various physical mechanisms including roof impact, viscous damping etc. forcing the sloshing to unsteady regimes) and defines a downshift ('hard spring') or upshift ('soft spring') of maximum wave amplitude response versus $T/T1$ relative to the exact linear response $T/T1 = 1$. This pair of jumps constitutes the hysteresis between two stable solutions. In accordance with the single dominant model by Faltinsen *et al.* (2000) the maximum downshift (upshift) is always restricted by vertical asymptote $T/T1 = T_*/T1$ found from the equation $m_1(h/l, T_*) = 0$. This bound is consistent with the fifth-order approximation by Waterhouse (1994) made for the near-critical depth case $m_1(h/l, 1) \approx 0$. However, there is no downshift (upshift) for the critical fluid depth case, where $m_1(h/l, 1) = 0$. The third- and fifth-order single dominant theories give then the maximal response for linear resonance $T/T1 = 1$.

The single dominant theory assumes the excitation amplitude and amplitude response to be very small and gives the trend of amplitude response with increasing the excitation amplitude. In particular, it shows that the intersection of the branches increases with excitation amplitude. For the 'soft-spring' (even if $m_1(h/l, 1)$ is very small) the turning point drifts up to the vertical asymptote $T_*/T1$ in the effective domain of the secondary resonance $i_2 = i(2, h/l)$. Since single dominant theory does not account for secondary resonance, the boundary $T_*/T1$ of the maximal upshift

https://doi.org/10.1017/S0022112000003311 Published online by Cambridge University Press

becomes questionable. We can instead use i_2 as boundary i_2 for maximal upshift. We expect the effect of the secondary resonance even for the lower fluid depths ('hard spring' response) when amplitudes are sufficiently large. It is then difficult to show the downshift (upshift).

Our calculation strategy for steady-state solutions is based on solving the initial Cauchy problem for adaptive modal system (3.1). A very small linear damping term $\alpha\sigma_i\dot{\beta}_i$ is incorporated into each ith modal equation, where α was varied from 0.005 to 10^{-6}–10^{-7}. The long time series will therefore give an approximation of steady-state solutions due to damping effects. Our estimate of the damping is based on the theory by Keulegan (1959) (maximal value $\alpha = 0.005$ is consistent with his prediction for the primary mode). The time integration normally started from zero initial conditions unless we expected two steady-state solutions in the hysteresis domain. The time integration procedure was then continued with initial conditions obtained from the previous simulation. This makes it possible to follow the branches using our computational scheme and, therefore, describe the hysteresis. Some discussion on that is given below. The maximum damping coefficient was used for the first time series. When the numerical solution attained a periodic structure, the damping coefficient was decreased by a factor of 10. The time to reach this periodical solution increases exponentially with decreasing α. This limits us to use uniformly small α. Only some isolated cases near turning points predictions were tested with $\alpha = 10^{-8}$–10^{-10}.

The mean time to reach a steady-state solution via our calculation scheme amounts to 30 min of real sloshing time on the model scale and depends on the excitation amplitude and frequency. An Adams–Bashforth–Moulton Predictor–Corrector integrator of varied order (from one to twelve) was used. The simulations were made on a Pentium-II 266 computer. The simulation time depends on the excitation parameters and damping and varied between 1/2 and 1/50 of real sloshing time in the experiments. This combined with Froude scaling of time implies that the simulations for full-scale conditions can be achieved in a considerably less time than the real time.

4.1. *Surge-excited resonant sloshing*

Surge-excited resonant sloshing in a rectangular tank with mean fluid depth close to the critical value $h/l = 0.3374$ was studied experimentally by Olsen & Johnsen (1975). Steady-state fluid response was compared with the third-order Moiseyev theory by Faltinsen (1974). This theory predicts infinite response as $T \to T1$ at the critical depth. If the higher-order Moiseyev-like theory by Waterhouse (1994) is used, the response will be finite. But the predicted amplitudes are much larger and unrealistic relative to the experiments by Olsen & Johnsen (1975) for the fluid depth/tank breadth ratio $h/l = 0.35$ presented in figure 5. We have tested third- and fifth-order asymptotic relations by Faltinsen (1974) and Waterhouse (1994) in our calculations to validate them with experimental data. Corresponding modal systems give a very large response in higher modes as $T \to T1$ in the case of figure 5. Large damping coefficients are then required to damp transients and to achieve a steady-state numerical solution. When decreasing these coefficients even small numerical error leads to a new series of large-amplitude transients. This means the hydrodynamic instability instead of the stable sloshing found in experiments. Since the response of higher modes becomes of the same order as the primary mode, it also means that the secondary resonance effective domain overlaps with the lowest mode resonance zone. We have therefore applied an adaptive method to this problem.

The numerical results from our calculation method are shown in figure 5. The calculation procedure has several stages. The first stage of the analysis was to locate

https://doi.org/10.1017/S0022112000003311 Published online by Cambridge University Press

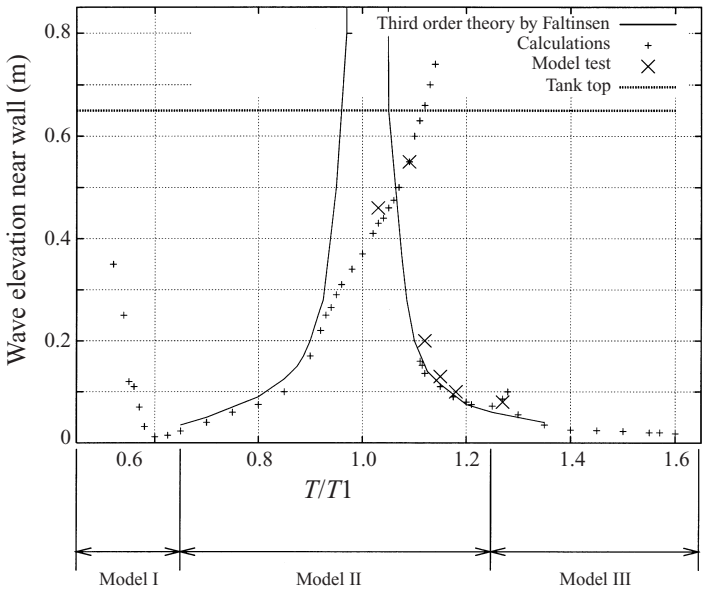


FIGURE 5. Wave elevation near the wall vs. the ratio of the period and the first natural period, $T/T1$. Rectangular tank in figure 2(*a*) with $h/l = 0.35$, $H/l = 0.025$. H is the surge excitation amplitude.

four possible resonances for $T/T1$ between 0.45 and 1.65. The primary resonances of the first and third mode occur at respectively $T/T1 = 1$ and $T/T1 = 0.55$. The secondary resonance of the second mode is predicted at $T/T1 = 1.28$. The secondary resonance of the third mode is at $T/T1 = 1.55$. Three models applicable for domains of different period were used. They are called Model I, II and III (it was ensured that the models overlap with each other in a small domain). Model I was used for $0.5 \leqslant T/T1 \leqslant 0.65$. The expected resonances are due to primary excitation of the third and first mode. They have the same main frequency response σ. No secondary resonance is expected. This leads to the relations $\beta_1 \sim \beta_3 = O(\epsilon^{1/3})$, and means that the secondary modes have the main harmonic 2σ. Such modes are $\beta_2 \sim \beta_6 = O(\epsilon^{2/3})$. Other modes (up to 9th) are considered as driven and of $O(\epsilon)$. The modal system based on (3.7) (Model II) was used for $0.6 \leqslant T/T1 \leqslant 1.28$. The modes $\beta_3, \beta_4, \beta_5, \beta_6$ were included as driven. If response is not too large, the modal system (3.7) gives the same results as for the third-order response by Faltinsen (1974) or by (3.4). When $T/T1 > 1.28$, the third-mode response was assumed to have the same order as β_1 and β_2 (Model III). The reason is the influence of the secondary resonance of the third mode at $T/T1 = 1.55$. Model III was used for $1.28 < T/T1 < 1.65$.

The calculations accounting for secondary resonances are in good agreement with experiments. They improve on the single dominant theoretical prediction between $0.9 < T/T1 < 1.11$ (primary resonance) and $1.21 < T/T1 < 1.32$ (secondary resonance of the second mode). In accordance with our calculations the maximum response is at $T/T1 = 1.11$ instead of the preliminary prediction $T/T1 = 1$. This gives an upshift of the maximum amplitude response in good agreement with experimental data. A local maximum is found experimentally and numerically at $T/T1 = 1.3$. This maximum response is caused by the secondary resonance phenomenon. Note that the computation strategy allows the upper branch to be followed up to very large amplitudes in the cases $T/T1 = 1.11$ and $T/T1 = 1.3$ when using the results of

https://doi.org/10.1017/S0022112000003311 Published online by Cambridge University Press

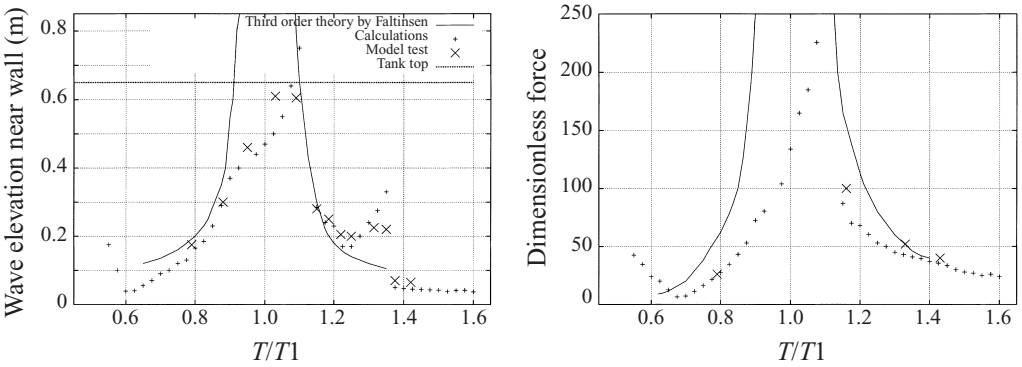


FIGURE 6. Wave elevation near the wall and dimensionless lateral force $1000F_x/(\rho g l^2 b)$ vs. $T/T1$. Rectangular tank in figure 2(*a*) with $h/l = 0.35$, $H/l = 0.05$. H is the surge excitation amplitude.

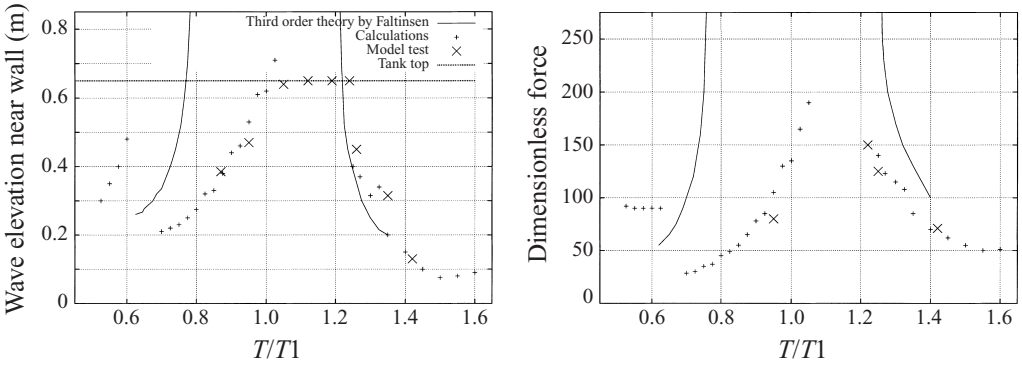


FIGURE 7. As figure 6 but with $H/l = 0.1$.

previous calculations as initial Cauchy conditions in new time series. Only numerical instability and the involvement of many secondary modes in resonance prevents us continuing the branch to infinity. For the case in figure 5 (Model II) these difficulties appear as wave amplitude tends to $1\,m$, corresponding to $T/T1 = 1.21$. On the other hand, we cannot move leftwards of $T/T1 = 1.11$ along the lower branch. The turning point limits us from doing this. The simulations then give a series of transients resulting in the stable steady solution on the upper branch. This means we cannot avoid a hysteresis effect occurring around $T/T1 = 1.11$ and $T/T1 = 1.3$ in the simulations. The increment periods in the experiment were probably too large to detect this hysteresis. In addition, the transient wave amplitudes will in reality cause a series of heavy roof impacts, which damp the system and eliminate large-amplitude steady-state waves for excitation periods higher than $T/T1 = 1.11$. The model presented does not account for roof impact.

Since the excitation amplitude is small in the case of figure 5, the local maximum at secondary resonance $T/T1 = 1.3$ is not too large. However, it increases with excitation amplitude H. Figures 6 and 7 present comparisons between experiments and calculations for larger excitation amplitudes. The tank and fluid depth is the same as used for figure 5. Both wave elevation near the tank wall and lateral fluid force are examined. (The symbol b used in the expression for dimensionless force is the tank length.) The simulation strategy in using Models I, II and III did not change. Our

https://doi.org/10.1017/S0022112000003311 Published online by Cambridge University Press

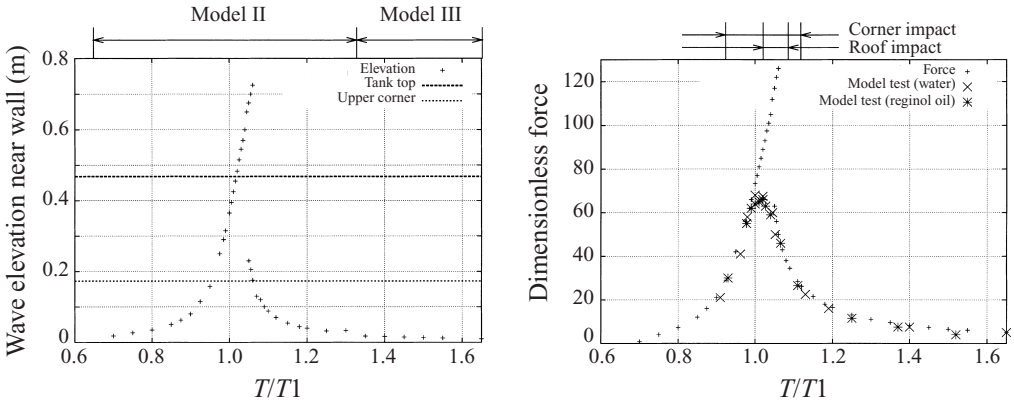


FIGURE 8. Wave elevation near the wall and dimensionless lateral force $1000F_x/(\rho g l^2 b)$ vs. $T/T1$. Prismatic tank in figure 2(*b*) with $h/l = 0.4$, $H/l = 0.01$. H is the surge excitation amplitude.

calculations show that the effective domain of secondary resonance increases with increasing excitation amplitude. It covers the range from 0.6 to 1.28 in figure 7. The jump in wave elevation response also increases at $T/T1 = 1.3$. The experiments and our calculations show that increasing the amplitude in figures 5 and 6 results in a small change of the upshift caused by the main resonance, but sufficient upshift near secondary resonance. Both upshifts become larger with increasing amplitude in the case of figure 7.

The effective domain of the secondary resonance by the third mode also increases. Since only odd modes contribute to the lateral force, the secondary resonance of the second mode is generally more important for wave elevation than for lateral force. However, for sufficiently large excitation amplitude the effect of secondary resonance also becomes important for lateral force. The reason is the inter-modal interaction between nearest odd modes β_1 and β_3 which, due to secondary resonance of the third mode, interact nonlinearly with each other and have the same order.

Our theory was also compared with experimental results for steady-state sloshing in the prismatic tank shown in figure 2(*b*). Figures 8 and 9 present the calculated and measured values of lateral force for small and non-small excitation amplitude respectively. This tank has a chamfered roof. Water impact on the tank roof was experimentally observed. We give therefore, as well as lateral force, the calculated wave elevation response. Two horizontal lines illustrate respectively the heights above the mean free surface of the lower point of the upper corner and the horizontal tank roof. Experiments for two different fluids are presented. This shows that viscosity is unimportant for horizontal forces.

The third-order steady-state theory by Faltinsen (1974) gave unrealistic predictions for both cases. The predicted force amplitudes in resonant conditions could for instance be 13 times larger than experiments in the case of figure 9. Our predictions are far more reasonable, especially for the small-amplitude excitation in figure 8. The single dominant theory by Faltinsen *et al.* (2000) gave unrealistic predictions for the largest amplitude responses. Fair agreement was obtained only for the smaller excitation amplitude in figure 8 away from the maximum response period domain.

The experiments as well as our theory predict that fluid hits the horizontal tank roof. This happens in small vicinity of the linear resonance for the case in figure 8 and in the period range $0.85 < T/T1 < 1.25$ for the case in figure 9. Rognebakke &

https://doi.org/10.1017/S0022112000003311 Published online by Cambridge University Press

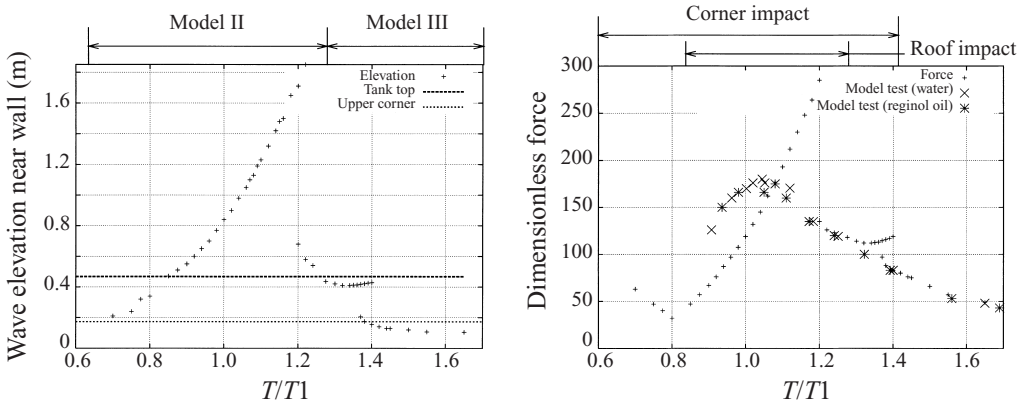


FIGURE 9. As figure 8 but with $H/l = 0.1$.

Faltinsen (2000) included tank roof impact in the single dominant theory by Faltinsen *et al.* (2000). They were able to simulate only the smaller excitation amplitude case. Their maximum predicted dimensionless force was 120, which is clearly larger than the prediction given by the adaptive method in this paper. However, the adaptive method clearly disagrees with experiment for the case in figure 9 when the horizontal fluid motion is in the opposite direction to forced tank motion, i.e. for $T/T1 < 1.14$. The detailed calculations by these adaptive models for ambient flows accounting for roof impact are given by Faltinsen & Rognebakke (2000). These studies have shown that damping due to impact improves the simulations. The disagreement shown in figure 9 then disappears.

4.2. *Pitch-excited resonant sloshing*

The experiments by Olsen & Johnsen (1975) and Olsen (1970) were used to validate the theory with pitch resonant excitation of steady-state sloshing. The experiments presented in figures 10, 11 and 12 were made with the rectangular tank shown in figure 2(*a*). Figure 10 gives computed and measured maximum wave amplitudes of steady-state sloshing for angular amplitude $\psi_0 = 0.1$ rad. Since the excitation amplitude is sufficiently small, the wave elevation never hits the roof in steady-state motion. However, the calculations show that 'beating' waves during transients sometimes have amplitude up to 1.6 times the breadth. Such transients can cause heavy roof impact. Our computational strategy did not differ from the previous cases. The domains of Models I, II and III are indicated for all the examples considered.

The theory is in good agreement with experiments in figure 10. The secondary resonance of the second mode is also well predicted. A jump between two branches occurs at $T/T1 = 1.111$. This value is the position of the turning point in our calculations. Since experiments show a value between these branches (point $J1$), it is believed that this is due to inaccurate modelling of damping. This will be more evident for a larger excitation amplitude. One could of course also state, by looking at this as an isolated case, that the error in predictions at the jump period is small and not larger than at other periods.

The minimum at $T/T1 = 0.74$ is not consistent with the minimum at $T/T1 = 0.6$ shown in figure 5 for the same fluid depth. The reason is the difference in the type of excitation. The modal approach gives the inhomogeneous periodic terms $P_m H\sigma^2 \cos\sigma t$ in the mth modal equation for surge excitation. The corresponding periodic term is

https://doi.org/10.1017/S0022112000003311 Published online by Cambridge University Press

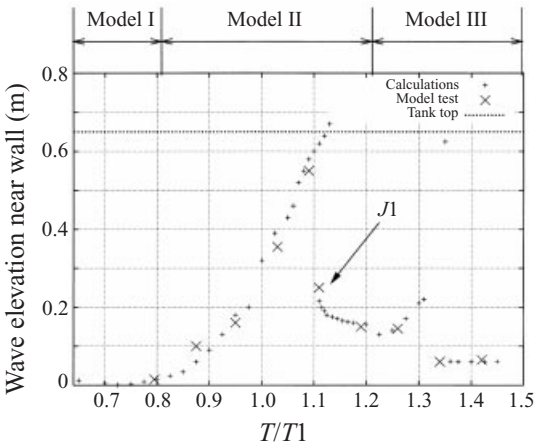


FIGURE 10. Wave elevation near the wall vs. $T/T1$. Rectangular tank in figure 2(a) with $h/l = 0.35$, $\psi_0 = 0.1$ rad. ψ_0 is pitch excitation amplitude.

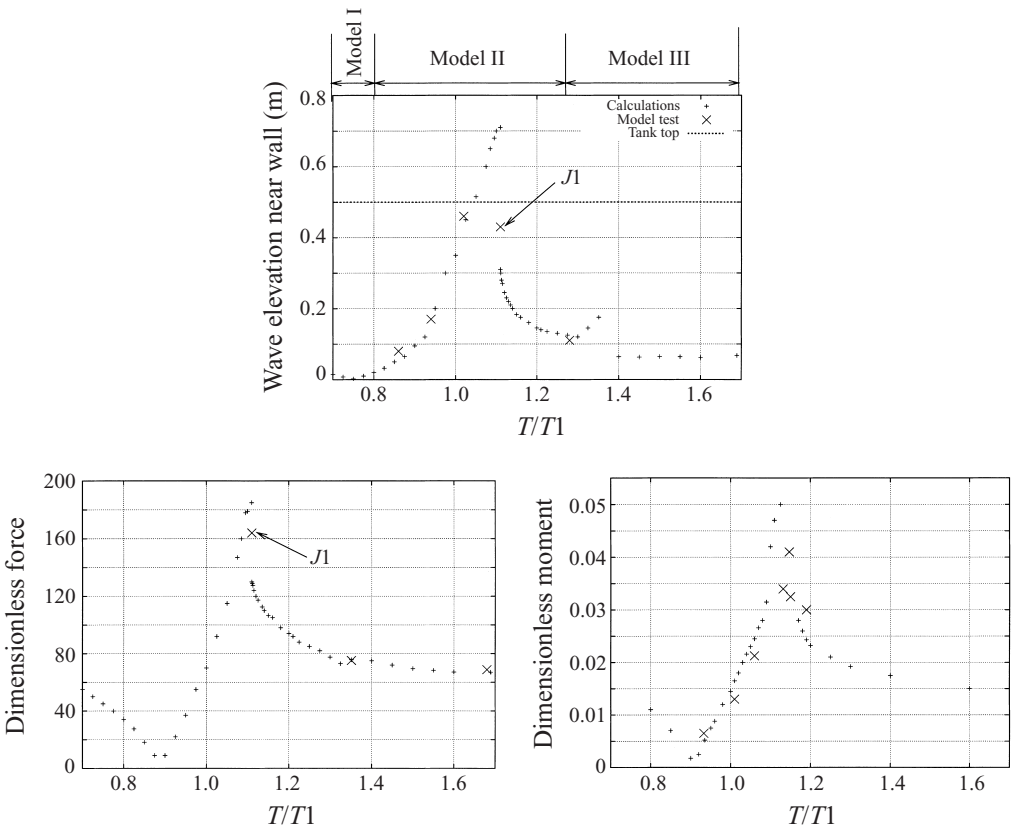


FIGURE 11. Wave elevation near the wall, dimensionless lateral force $1000F_x/(\rho g l^2 b)$ and dimensionless pitch moment $M/(\rho g l^3 b)$ with respect to rotation axis vs. $T/T1$. Rectangular tank in figure 2(a) with $h/l = 0.5, \psi_0 = 0.1$ rad. The measurements of lateral force and pitch moment were made by Olsen (1970, personal communication).

https://doi.org/10.1017/S0022112000003311 Published online by Cambridge University Press

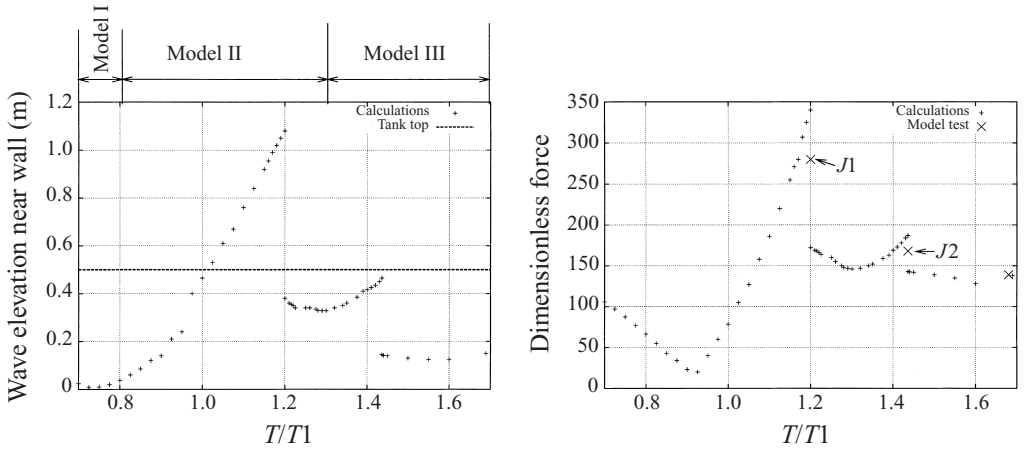


FIGURE 12. Wave elevation near the wall and dimensionless lateral force $1000F_x/(\rho g l^2 b)$ with respect to rotation axis vs. $T/T1$. Rectangular tank with $l = 1.0$ m, $h/l = 0.5$, $\psi_0 = 0.2$ rad. The measurements of lateral force were made by Olsen (1970, personal communication).

$P_m\psi_o(z_0-(2l/\pi m)\tanh((m\pi/2l)h)+(g/\sigma^2))\sigma^2\cos\sigma t$ for pitch excitation, where P_m is a function of fluid depth. The expression in the parentheses depends on z_0 (z-coordinate of rotation axis), σ (excitation frequency), fluid depth h and tank breadth l. There exist values of z_0 and σ that can cancel this periodic term in the modal equation for the first mode ($m = 1$). Then this mode is not excited and we should consider the sloshing as due to inter-modal interaction with other modes.

Figure 11 presents calculated and measured values of steady-state wave elevation, lateral force and pitch moment, for $h/l = 0.5$ which is far from the critical depth. Faltinsen (1974) also compared steady-state wave elevation with experimental recordings for this case and showed good predictions for selected periods. *A priori* we might have expected the largest response close to critical depth, i.e. in figure 10. But the theoretical and experimental amplitude responses are larger in figure 11. The reason is the increase of angular excitation due to increased distance between rotating axis and mean free surface. This leads to larger values of the pitch excitation term $P_m\psi_0\sigma^2(z_0-(2l/\pi m)\tanh((m\pi/2l)h)+(g/\sigma^2))\cos\sigma t$ in the mth modal equation of (3.1).

The theory agrees well with experiments in the case of figure 11. But the calculations do not predict the experimental response found at the jump period $T/T1 = 1.111$ (point $J1$). This is believed to be due to damping. The calculations describe the effect of secondary resonance of the second mode on the lateral force. This influence is very small in figure 10. When the excitation amplitude is increased to 0.2 rad, this secondary resonance gives an additional jump (point $J2$) at $T/T1 = 1.45$ (see figure 12). We note that the experimental values $J1$ and $J2$ are not predicted well. The reason has been previously discussed.

We also tried to validate the theory for a pitch-excited prismatic tank. An appropriate example was found in the paper by Mikelis *et al.* (1984) (see also Delft University Report 1983). This prismatic tank is presented in figure 2(*d*). Figure 13 gives calculated and measured hydrodynamic pitch moments. Models I, II and III were used in different forced excitation frequency domains as indicated in the figure caption. They are in good agreement with experiments except in the frequency range where the calculated wave elevation indicates roof impact. The response is presented

https://doi.org/10.1017/S0022112000003311 Published online by Cambridge University Press

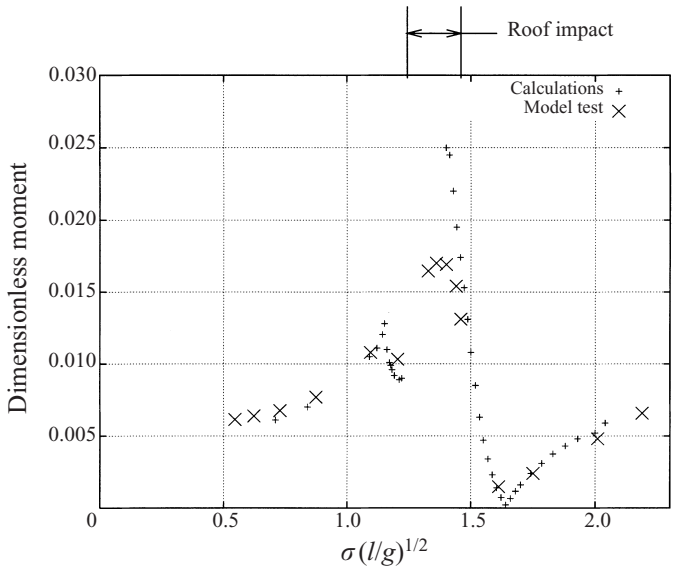


FIGURE 13. Dimensionless pitch moment $M/(\rho g l^3 b)$ with respect to rotation axis vs. dimensionless forced excitation frequency $\sigma\sqrt{l/g}$, where σ has dimension [rad s^{-1}]. Prismatic tank in figure 2(*d*) with $h/l = 0.182$, $\psi_0 = 0.1$ rad. Models I, II and III were respectively used in domains $1.75 < \sigma\sqrt{l/g} < 2.5$, $1.19 < \sigma\sqrt{l/g} < 1.75$ and $0.6 < \sigma\sqrt{l/g} < 1.19$.

as function of $\sigma\sqrt{l/g}$ instead of $T/T1$. This is convenient when studying asymptotic moment values for $\sigma \to 0$, caused by the hydrostatic moment on the inclined tank. Our computations for $\sigma \to 0$ give the dimensionless value 0.005 compared to the experimental value 0.00518. (The calculations for small σ were done with a model of seven nonlinearly coupled modes based on (3.1).) The reason for this small difference is simply our modal presentation of the free surface, which means that a static inclined tank in our approximation has non-planar free surface.

4.3. *Sloshing in a tank with small fluid depth*

We tested the above adaptive procedure for different values of fluid depth by comparing with experiments by Rognebakke (1999). Models I, II and III gave well predicted values of wave responses in the period domain of the primary mode for fluid depth $h/l \geqslant 0.24$. When $h/l < 0.24$, these models could not cover this period domain completely if excitation amplitude is sufficiently large. That is why we do not present the comparison with experiments by Olsen & Johnsen (1975) for pitch-excited resonant sloshing with $h/l = 0.2, \psi_0 = 0.1$ rad in the rectangular tank in figure 2(*a*). This fluid depth is not sufficiently small to use shallow water theory. However, in the framework of our adaptive method we have speculatively tested some different possible shallow water asymptotics including asymptotics given by Ockendon *et al.* (1986) ($\beta_i = O(\epsilon^{1/2})$ or $\beta_i = O(\epsilon^{1/4})$). Test calculations were made with six modes in (3.1). In both cases there exist some excitation period domains where either calculated responses were not consistent with experiments or the modal system (3.4) gave only a few seconds of real time integration before numerical problems occurred. The reason is believed to be the weak convergence of the modal expression for the free surface. A small change of excitation needs a new ordering between modes and gives different dominating harmonics in each mode. One way to explain this is by the change of wave patterns

https://doi.org/10.1017/S0022112000003311 Published online by Cambridge University Press

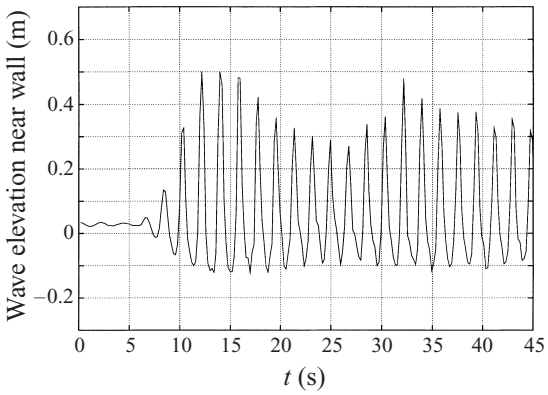


FIGURE 14. Measured surface elevation near the wall. Rectangular tank in figure 2(*c*) with $h/l = 0.173, H/l = 0.029, T/T1 = 0.8508$. H is the surge excitation amplitude.

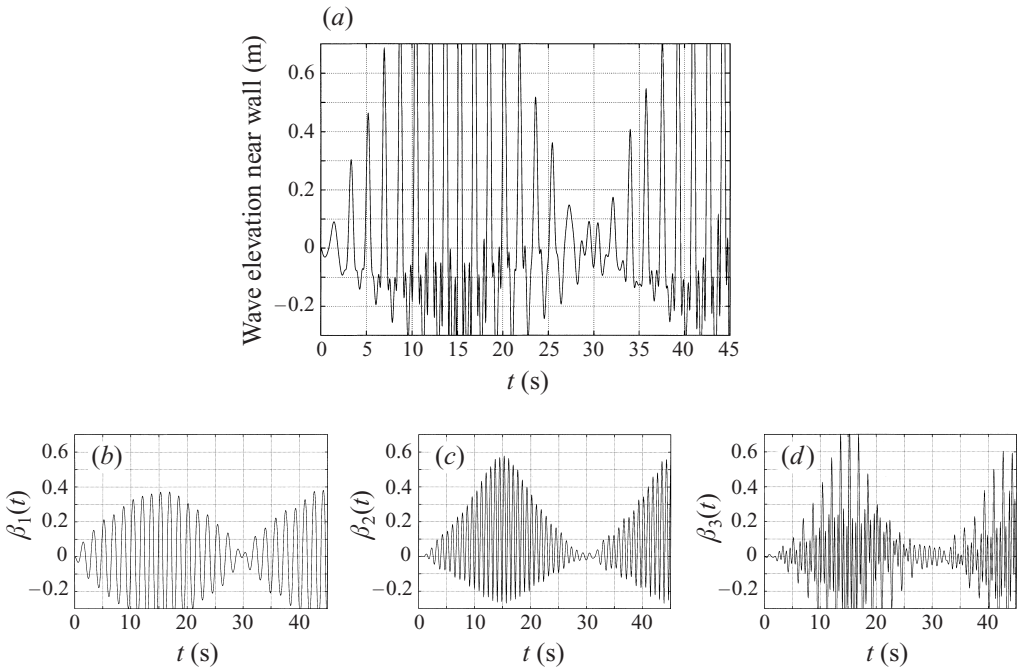


FIGURE 15. Calculated free surface elevation near the wall. (*a*) Model of Faltinsen *et al.* (2000). (*b–d*) Modal system (3.4): contributions from modes 1, 2 and 3 respectively. Rectangular tank in figure 2(*c*) with $h/l = 0.173$, $H/l = 0.029$, $T/T1 = 0.8508$.

relative to the finite fluid depth case with $h/l \geqslant 0.24$. When the fluid depth is small, wave patterns associated with 'travelling' waves and 'run-up' phenomena occur. Many modes are required to approximate such wave profiles in a Fourier series expressing standing wave-type solutions (1.1). Damping due to run-up may also matter.

An example below illustrates the main difficulties associated with modelling sloshing for small fluid depth. It is based on resonant sloshing experiments in the rectangular tank shown in figure 2(*d*). The free surface elevation recording at wave probe FS3 is presented in figure 14. The modal system (3.4) gives wave elevation as shown in figure 15. The contribution to wave elevation from each mode is also presented in figure

https://doi.org/10.1017/S0022112000003311 Published online by Cambridge University Press

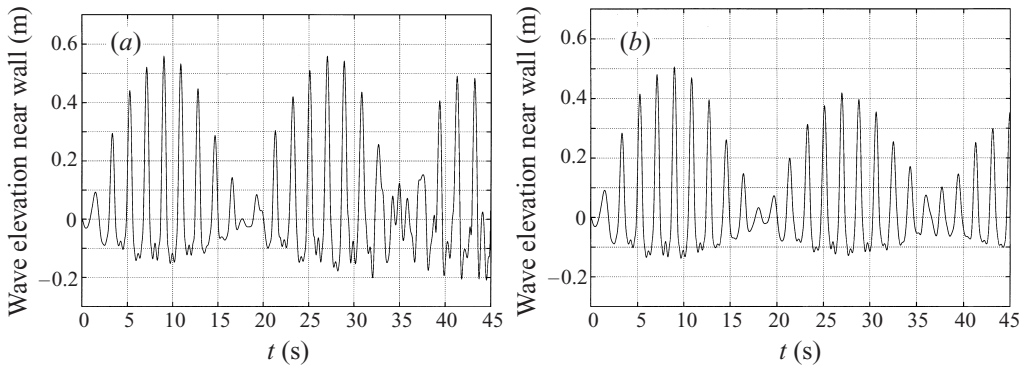


FIGURE 16. Calculated free surface elevation near the wall. Rectangular tank in figure 2(*c*) with $h/l = 0.173, H/l = 0.029, T/T1 = 0.8508$. H is the surge excitation amplitude. Modal system includes $\beta_1 = O(\epsilon^{1/3}), \beta_2 = O(\epsilon^{1/3}), \beta_3 = O(\epsilon^{1/3}), \beta_4 = O(\epsilon^{2/3})$. (*a*) Adaptive model, no damping. (*b*) Damping is based on the theory by Keulegan (1959).

15. Similar results were presented by Faltinsen *et al.* (2000). These numerical results suggest that inter-modal resonances between the primary resonance at $T/T1 = 1$, the secondary resonance of the second mode at $T/T1 = 1.1446$, the direct resonance of the third mode at $T/T1 = 0.56$ and the secondary resonance of the third mode at $T/T1 = 1.32275$ are important. Since these resonance periods are very similar, they should all be accounted for.

Harmonic analysis of the contributions gives the main harmonic $H_1 \cos \sigma t$ in the primary mode and the main harmonic $H_2 \cos 2\sigma t$ in the second mode. The graph 'Mode 3' in figure 15(*d*) shows that direct and secondary resonance give two main harmonics, $H_3 \cos \sigma t$ and $H_4 \cos 3\sigma t$, for the third mode. The reason is that $T/T1 = 0.8508$ is equally close to 0.56 and 1.32275. Thus, three modes should be considered having the same order, $O(\epsilon^{1/3})$. One of the modes has two main harmonics. This contradicts our previous assumption in finite fluid depth cases, and means that three nonlinear modal equations give three equations with four unknown variables H_1, H_2, H_3 and H_4 in a steady-state analysis. A way to avoid this contradiction is to add a mode at $O(\epsilon^{2/3})$ that interacts with dominant modes. This mode will be of included nonlinearly in the equations but its main harmonics will be of higher order than the dominant $\beta_1, \beta_2, \beta_3$. We used for time simulation an adaptive system with $\beta_1 \sim \beta_2 \sim \beta_3 = O(\epsilon^{1/3}), \beta_4 = O(\epsilon^{2/3})$. The calculated wave elevation is shown in figure 16(*a*). It gives a realistic approximation for both minimum and maximum wave elevation and 'beating' period. However, the higher modes have 'high harmonics' noise. This causes numerical problems in very long time simulations. However, these high modes are believed to be highly damped due to energy dissipation. We have therefore incorporated in the modal system some additional linear damping terms $\alpha\sigma\dot{\beta}_\mu$. The damping coefficient α introduced was not high, since it was based on the theory by Keulegan (1959) for the primary mode. Damping improves numerical integration. The calculated wave elevation is presented in figure 16(*b*).

A detailed study of the experiments for this fluid depth shows that wave run-up near the vertical wall occurs for all excitation periods in the effective domain of primary resonance. A typical wave profile is presented in figure 17. The maximum length and thickness of the vertical wall jet depends on excitation period. This jet cannot be described in the context of Fourier approximation (1.1). Mathematical

https://doi.org/10.1017/S0022112000003311 Published online by Cambridge University Press

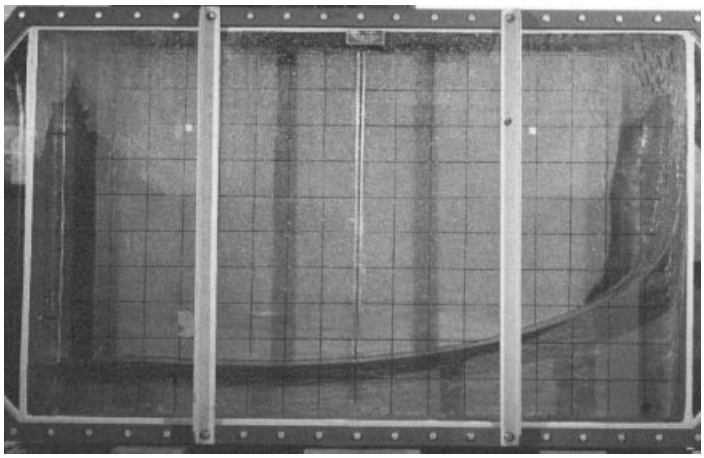


FIGURE 17. Run-up phenomenon. Resonant sloshing in the rectangular tank in figure 2(*d*). Surge excitation. Experiments by Rognebakke (1999).

singularity will occur at the body-fluid system contact point. This implies that a matching with a local solution at the contact point may be necessary.

5. Conclusions

Two-dimensional nonlinear sloshing in a rectangular tank is analytically studied. Irrotational flow of incompressible fluid, infinite tank roof height and no overturning waves are assumed.

The basis of the theory is an infinite-dimensional system of nonlinear ordinary differential equations coupling generalized coordinates β_i of a modal system. This is derived from a variational procedure by Faltinsen *et al.* (2000). By assuming the fluid response to be small relative to fluid depth and tank breadth this modal system is asymptotically reduced to an infinite-dimensional system of ordinary differential equations with polynomial nonlinearity of fifth order in β_i. It also contains third-order terms coupling β_i and time-varying functions describing rigid body motion. No ordering among the β_i is assumed. The coefficients of this system are unique functions of fluid depth. However, the number of non-zero coefficients increases drastically with increasing dimensions.

The surge and pitch excitation of the tank is considered. The tank is forced to oscillate with period in the vicinity of the highest natural period of fluid motion. By introducing asymptotic relations between the β_i the system derived can be detuned to particular cases of nonlinear sloshing occurring due to direct and secondary resonances. Secondary resonance is taken to mean that higher harmonics in the fluid motion cause resonant motion at natural periods other than primary resonance periods.

The theory based on Moiseyev-like inter-modal relations by Faltinsen *et al.* (2000) is a special case. This asymptotic theory is invalid when the excitation amplitude is not very small, and the fluid depth is close to critical or shallow. This is caused by the large-amplitude response in both the primary and a few higher modes. It is demonstrated that inter-modal relations depend on excitation amplitude, period and fluid depth. If each mode has only one lowest-order harmonic, the rational choice of these relations is motivated by locating primary and secondary resonance periods. The

https://doi.org/10.1017/S0022112000003311 Published online by Cambridge University Press

method has been validated by comparing with model tests. Adaptive procedures have been established for all excitation periods as long as the mean fluid depth is larger than 0.24 times the tank breadth. Steady-state results for wave elevation, horizontal force and pitch moment due to forced surge and pitch excitation are validated except when heavy roof impact occurs. Different stable branches of the analytical solutions are located.

When $h/l < 0.24$ and depth is not shallow, good agreement with experiments has been achieved for isolated excitation periods. An example for $h/l = 0.173$, where the previous model by Faltinsen *et al.* (2000) failed, demonstrated this. When the fluid depth is small, many modes have the same order and each mode may have more than one main harmonic. Then the convergence of modal presentation (1.1) can fail and a pure modal technique using the natural modes is questionable.

The authors are grateful to H. Olsen for providing the unpublished measured data on lateral force and pitch moment in figures 11 and 12. A. N. T. is supported by the Strong Point Centre on Hydroelasticity at NTNU/SINTEF in Trondheim, Norway.

Appendix A. The tensors introduced

The set of tensors $\boldsymbol{\Lambda}$ is given by

$$\Lambda^{(0)}_{ij} = \begin{cases} 2 & i = j = 0 \\ \delta_{ij} & \text{otherwise} \end{cases} \tag{A 1}$$

where

$$\delta_{ij} = \begin{cases} 1, & i = j \\ 0, & i \neq j \end{cases}$$

is the Kronecker symbol. The following recurrence formulas have been obtained:

$$\left.\begin{aligned} \Lambda^{(1)}_{nkj} &= \Lambda^{(0)}_{|n-k|j} + \Lambda^{(0)}_{|n+k|j}, \quad \Lambda^{(2)}_{nkjp} = \Lambda^{(1)}_{|n-k|jp} + \Lambda^{(1)}_{|n+k|jp}, \\ \Lambda^{(3)}_{nkjpq} &= \Lambda^{(2)}_{|n-k|jpq} + \Lambda^{(2)}_{|n+k|jpq}, \quad \Lambda^{(4)}_{nkjpqi} = \Lambda^{(3)}_{|n-k|jpqi} + \Lambda^{(3)}_{|n+k|jpqi}; \end{aligned}\right\} \tag{A 2}$$

and

$$\left.\begin{aligned} \Lambda^{(-1)}_{nk,i} &= \Lambda^{(0)}_{|n-k|i} - \Lambda^{(0)}_{|n+k|i}, \quad \Lambda^{(-2)}_{nk,ij} = \Lambda^{(1)}_{|n-k|ij} - \Lambda^{(1)}_{|n+k|ij}, \\ \Lambda^{(-3)}_{nk,ijp} &= \Lambda^{(2)}_{|n-k|ijp} - \Lambda^{(2)}_{|n+k|ijp}, \quad \Lambda^{(-4)}_{nk,ijpq} = \Lambda^{(3)}_{|n-k|ijpq} - \Lambda^{(3)}_{|n+k|ijpq}. \end{aligned}\right\} \tag{A 3}$$

The sets of $\boldsymbol{X}$ and $\boldsymbol{Y}$ tensors are defined by

$$X^{(0)}_i = (-1)^i - 1, \quad X^{(-0)}_\mu = (-1)^\mu + 1, \tag{A 4}$$

$$X^{(1)}_{ik} = \frac{X^{(0)}_{|i+k|}}{(i+k)^2} + \frac{X^{(0)}_{|i-k|}}{(i-k)^2}\bigg|_{i-k\neq 0}, \quad X^{(2)}_{ikp} = X^{(1)}_{i|k-p|} + X^{(1)}_{i|k+p|}; \tag{A 5}$$

$$Y^{(1)}_{i,k} = \frac{X^{(0)}_{i+k}}{i+k} + \frac{X^{(0)}_{i-k}}{i-k}\bigg|_{i-k\neq 0}, \quad Y^{(2)}_{i,kp} = Y^{(1)}_{i,|k-p|} + Y^{(1)}_{i,k+p}. \tag{A 6}$$

Appendix B. The modal system in symmetric form

The $\boldsymbol{d}$ and $\boldsymbol{t}$ tensors are not symmetric for the complete set of indexes. It is important to note that $\boldsymbol{d}$ are not symmetric in $b\,c\,d\,f$ and $\boldsymbol{t}$ in $c\,d\,f$, since these coefficients are

https://doi.org/10.1017/S0022112000003311 Published online by Cambridge University Press

near the products in β and their derivatives. In order to obtain analytical symmetric structure we rewrite (3.1) in the form

$$\sum_{a=1}^{N}\ddot{\beta}_a(\delta_{am}+\sum_{b=1}^{N}\beta_b D1^m(a,b)+\sum_{b=1}^{N}\sum_{c=1}^{b}\beta_b\beta_c D2^m(a,b,c)$$
$$+\sum_{b=1}^{N}\sum_{c=1}^{b}\sum_{d=1}^{c}\beta_b\beta_c\beta_d D3^m(a,b,c,d)$$
$$+\sum_{b=1}^{N}\sum_{c=1}^{b}\sum_{d=1}^{c}\sum_{f=1}^{d}\beta_b\beta_c\beta_d D4^m(a,b,c,d,f)\beta_f)+\sum_{a=1}^{N}\sum_{b=1}^{a}\dot{\beta}_a\dot{\beta}_b T0^m(a,b)$$
$$+\sum_{a=1}^{N}\sum_{b=1}^{a}\sum_{c=1}^{N}\dot{\beta}_a\dot{\beta}_b\beta_c T1^m(a,b,c)+\sum_{a=1}^{N}\sum_{b=1}^{a}\sum_{c=1}^{N}\sum_{d=1}^{c}\dot{\beta}_a\dot{\beta}_b\beta_c\beta_d T2^m(a,b,c,d)$$
$$+\sum_{a=1}^{N}\sum_{b=1}^{a}\sum_{c=1}^{N}\sum_{d=1}^{c}\sum_{f=1}^{d}T3^m(a,b,c,d,f)\dot{\beta}_a\dot{\beta}_b\beta_c\beta_d\beta_f+\sigma_m^2\beta_m$$
$$+P_m(\dot{v}_{0x}-g\psi)+\dot{\omega}Q_m L_m^{(0)}=0, \tag{B 1}$$

where

$$D1^m(a,b)=d^{1,m}_{a,b},$$

$$D2^m(a,b,c)=\begin{cases} d^{2,m}_{a,b,b}, & b=c \\ d^{2,m}_{a,b,c}+d^{2,m}_{a,c,b}, & b\neq c, \end{cases}$$

$$D3^m(a,b,c,d)=\begin{cases} d^{3,m}_{a,b,b,b}, & b=c=d \\ d^{3,m}_{a,b,b,d}+d^{3,m}_{a,b,d,b}+d^{3,m}_{a,d,b,b}, & b=c,\ c\neq d \\ d^{3,m}_{a,b,c,c}+d^{3,m}_{a,c,b,c}+d^{3,m}_{a,c,c,b}, & b\neq c,\ c=d \\ d^{3,m}_{a,b,c,d}+d^{3,m}_{a,b,d,c}+d^{3,m}_{a,c,b,d}+d^{3,m}_{a,c,d,b}+d^{3,m}_{a,d,b,c}+d^{3,m}_{a,d,c,b}, & b\neq c,\ c\neq d, \end{cases}$$

$$T0^m(a,b)=\begin{cases} t^{0,m}_{a,a} & a=b \\ t^{0,m}_{a,b}+t^{0,m}_{b,a} & a\neq b, \end{cases}$$

$$T1^m(a,b,c)=\begin{cases} t^{1,m}_{a,a,c} & a=b \\ t^{1,m}_{a,b,c}+t^{0,m}_{b,a,c} & a\neq b, \end{cases}$$

$$T2^m(a,b,c,d)=\begin{cases} t^{2,m}_{a,a,c,c} & a=b,\ c=d \\ t^{2,m}_{a,b,c,c}+t^{2,m}_{b,a,c,c} & a\neq b,\ c=d \\ t^{2,m}_{a,a,c,d}+t^{2,m}_{a,a,d,c} & a=b,\ c\neq d \\ t^{2,m}_{a,b,c,d}+t^{2,m}_{b,a,c,d}+t^{2,m}_{a,b,d,c}+t^{2,m}_{b,a,d,c} & a\neq b,\ c\neq d, \end{cases}$$

https://doi.org/10.1017/S0022112000003311 Published online by Cambridge University Press

$$
D4^m(a,b,c,d,f)=\begin{cases}
d^{4,m}_{a,b,b,b,b}, & b=c=d=f\\
d^{4,m}_{a,b,b,b,f}+d^{4,m}_{a,b,b,f,b}+d^{4,m}_{a,b,f,b,b}+d^{4,m}_{a,f,b,b,b}, & b=c=d,\ d\neq f\\
d^{4,m}_{a,c,c,b,c}+d^{4,m}_{a,c,c,c,b}+d^{4,m}_{a,b,c,c,c}+d^{4,m}_{a,c,b,c,c}, & b\neq c,\ c=d=f\\
d^{4,m}_{a,c,c,d,d}+d^{4,m}_{a,d,d,c,c}+d^{4,m}_{a,c,d,c,d}+d^{4,m}_{a,d,c,d,c}\\
\quad+d^{4,m}_{a,c,d,d,c}+d^{4,m}_{a,d,c,c,d}, & b=c,\ c\neq d,\ d=f\\
d^{4,m}_{a,b,b,d,f}+d^{4,m}_{a,b,b,f,d}+d^{4,m}_{a,b,d,f,b}+d^{4,m}_{a,b,f,d,b}\\
\quad+d^{4,m}_{a,d,f,b,b}+d^{4,m}_{a,f,d,b,b}+d^{4,m}_{a,f,b,b,d}+d^{4,m}_{a,d,b,b,f}\\
\quad+d^{4,m}_{a,b,d,b,f}+d^{4,m}_{a,b,f,b,d}+d^{4,m}_{a,f,b,d,b}+d^{4,m}_{a,d,b,f,b}, & b=c,\ c\neq d,\ d\neq f\\
d^{4,m}_{a,c,c,b,f}+d^{4,m}_{a,c,c,f,b}+d^{4,m}_{a,c,b,f,c}+d^{4,m}_{a,c,f,b,c}\\
\quad+d^{4,m}_{a,b,f,c,c}+d^{4,m}_{a,f,b,c,c}+d^{4,m}_{a,f,c,c,b}+d^{4,m}_{a,b,c,c,f}\\
\quad+d^{4,m}_{a,c,b,c,f}+d^{4,m}_{a,c,f,c,b}+d^{4,m}_{a,f,c,b,c}+d^{4,m}_{a,b,c,f,c}, & b\neq c,\ c=d,\ d\neq f\\
d^{4,m}_{a,f,f,b,c}+d^{4,m}_{a,f,f,c,b}+d^{4,m}_{a,f,b,c,f}+d^{4,m}_{a,f,c,b,f}\\
\quad+d^{4,m}_{a,b,c,f,f}+d^{4,m}_{a,c,b,f,f}+d^{4,m}_{a,b,f,f,c}+d^{4,m}_{a,c,f,f,b}\\
\quad+d^{4,m}_{a,f,c,f,b}+d^{4,m}_{a,f,b,f,c}+d^{4,m}_{a,b,f,c,f}+d^{4,m}_{a,c,f,b,f}, & b\neq c,\ c\neq d,\ d=f\\
d^{4,m}_{a,b,c,d,f}+d^{4,m}_{a,c,b,d,f}+d^{4,m}_{a,b,c,f,d}+d^{4,m}_{a,c,b,f,d}\\
\quad+d^{4,m}_{a,b,d,f,c}+d^{4,m}_{a,c,d,f,b}+d^{4,m}_{a,b,f,d,c}+d^{4,m}_{a,c,f,d,b}\\
\quad+d^{4,m}_{a,d,f,c,b}+d^{4,m}_{a,f,d,c,b}+d^{4,m}_{a,d,f,b,c}+d^{4,m}_{a,f,d,b,c}\\
\quad+d^{4,m}_{a,b,d,c,f}+d^{4,m}_{a,c,d,b,f}+d^{4,m}_{a,b,f,c,d}+d^{4,m}_{a,c,f,b,d}\\
\quad+d^{4,m}_{a,d,c,f,b}+d^{4,m}_{a,f,b,d,c}+d^{4,m}_{a,d,b,f,c}+d^{4,m}_{a,f,b,d,c}\\
\quad+d^{4,m}_{a,d,b,c,f}+d^{4,m}_{a,f,c,b,d}+d^{4,m}_{a,d,c,b,f}+d^{4,m}_{a,f,c,b,d}, & b\neq c,\ c\neq d,\ d\neq f,
\end{cases}
$$

$$
T3^m(a,b,c,d,f)=\begin{cases}
t^{3,m}_{a,a,c,c,c} & a=b,\ c=d=f\\
t^{3,m}_{a,a,c,c,f}+t^{3,m}_{a,a,c,f,c}+t^{3,m}_{a,a,f,c,c} & a=b,\ c=d,\ d\neq f\\
t^{3,m}_{a,a,c,d,d}+t^{3,m}_{a,a,d,c,d}+t^{3,m}_{a,a,d,d,c}\\
\quad+t^{3,m}_{a,a,c,d,f}+t^{3,m}_{a,a,c,f,d}+t^{3,m}_{a,a,d,c,f} & a=b,\ c\neq d,\ d=f\\
\quad+t^{3,m}_{a,a,d,f,c}+t^{3,m}_{a,a,f,c,d}+t^{3,m}_{a,a,f,d,c} & a=b,\ c\neq d,\ d\neq f\\
t^{3,m}_{a,b,c,c,c}+t^{3,m}_{b,a,c,c,c} & a\neq b,\ c=d=f\\
t^{3,m}_{a,b,c,c,f}+t^{3,m}_{a,b,c,f,c}+t^{3,m}_{b,a,c,c,f}+t^{3,m}_{b,a,c,f,c}\\
\quad+t^{3,m}_{a,b,f,c,c}+t^{3,m}_{b,a,f,c,c} & a\neq b,\ c=d,\ d\neq f\\
t^{3,m}_{a,b,c,d,d}+t^{3,m}_{a,b,d,c,d}+t^{3,m}_{b,a,c,d,d}+t^{3,m}_{b,a,d,c,d}\\
\quad+t^{3,m}_{a,b,d,d,c}+t^{3,m}_{b,a,d,d,c} & a\neq b,\ c\neq d,\ d=f\\
t^{3,m}_{a,b,c,d,f}+t^{3,m}_{a,b,c,f,d}+t^{3,m}_{b,a,c,d,f}+t^{3,m}_{b,a,c,f,d}\\
\quad+t^{3,m}_{a,b,d,c,f}+t^{3,m}_{b,a,d,c,f}+t^{3,m}_{a,b,d,f,c}+t^{3,m}_{b,a,d,f,c}\\
\quad+t^{3,m}_{a,b,f,c,d}+t^{3,m}_{a,b,f,d,c}+t^{3,m}_{b,a,f,c,d}+t^{3,m}_{b,a,f,d,c} & a\neq b,\ c\neq d,\ d\neq f.
\end{cases}
$$

https://doi.org/10.1017/S0022112000003311 Published online by Cambridge University Press

REFERENCES

Abramson, H. N., Bass, R. L., Faltinsen, O. M. & Olsen, H. A. 1974 Liquid slosh in LNG Carriers. In *Tenth Symp. on Naval Hydrodynamics, June 24–28, 1974, Cambridge, Massachusetts* (ed. R. D. Cooper & S. W. Doroff). ACR-204, pp. 371–388. Office of Naval Research – Dept of the Navy, Arlington, Va., USA.

Cocciaro, B., Faeti, S. & Nobili, M. 1991 Capillary effect on surface gravity waves in cylindrical container: wetting boundary conditions. *J. Fluid Mech.* **231**, 325–343.

Delft University Rep. 583-O. 1983 *Roll moments due to free surface.* Technische Hogeschool Delft. Afdeling der Maritieme Techniek. Laboratorium voor Scheepshydromechanica. Orderno. O-1683. Reportno. 583-O. May 1983. Vakgroep Sheepshyhydromechanica. 24pp.

Eurosloshi: 1995 *Experimental and Numerical Analysis of Sloshing and Impact Loads.* Synthesis Report for Publication. Project Coordinator: M. Dogliani, Project BE–4354, 26/04/01.

Faltinsen, O. M. 1974 A nonlinear theory of sloshing in rectangular tanks. *J. Ship. Res.* **18**, 224–241.

Faltinsen, O. M. & Rognebakke, O. F. 1999 Sloshing and slamming in tanks. In *Hydronav'99.–Manoeuvering'99 Gdansk–Ostroda, 1999, Poland.*

Faltinsen, O. M. & Rognebakke, O. F. 2000 Sloshing. *NAV 2000. Proc. Intl Conf. on Ship and Shipping Research, Venice, 19–22 September, 2000, Italy* (ed. J. Szantyr, L. Kobylinski, J. Nowacki, W. A. Misiag & J. Bielánski). Dept Ship Hydro., Technical Univ. Gdańsk, Poland.

Faltinsen, O. M., Rognebakke, O. F., Lukovsky, I. A. & Timokha, A. N. 2000 Multidimensional modal analysis of nonlinear sloshing in a rectangular tank with finite water depth. *J. Fluid Mech.* **407**, 201–234.

Feschenko, S. F., Lukovsky, I. A., Rabinovich, B. I. & Dokuchaev, L.V. 1969 *Methods for Determining Added Fluid Mass in Mobile Cavities.* Kiev: Naukova dumka (in Russian).

Henderson, D. M. & Miles, J. W. 1991 Faraday waves in 2 : 1 internal resonance. *J. Fluid Mech.* **222**, 449–470.

Keulegan, G. H. 1959 Energy dissipation in standing waves in rectangular basin. *J. Fluid Mech.* **6**, 33–50.

Lukovsky, I. A. 1976 Variational method in the nonlinear problems of the dynamics of a limited liquid volume with free surface. In *Oscillations of Elastic Constructions with Liquid*, pp. 260–264. Moscow: Volna (in Russian).

Lukovsky, I. A. 1990 *Introduction to Nonlinear Dynamics of a Solid Body with a Cavity Including a Liquid.* Kiev: Naukova dumka (in Russian).

Lukovsky, I. A. & Timokha, A. N. 1995 *Variational Methods in Nonlinear Dynamics of a Limited Liquid Volume.* Kiev: Institute of Mathematics (in Russian).

Marti, J. T. 1986 *Introduction to Sobolev Spaces and Finite Element Solution of Elliptic Boundary Value Problems.* Computational Mechanics and Applications. Academic.

Mikelis, N. E., Miller, J. K. & Taylor, K. V. 1984 Sloshing in partially filled liquid tanks and its effect on ship motions: numerical simulations and experimental verification. *The Royal Institution of Naval Architects, Spring Meeting 1984, Paper No.* 7. 11pp.

Miles, J. W. 1976 Nonlinear surface waves in closed basins. *J. Fluid Mech.* **75**, 419–448.

Miles, J. W. 1984*a* Internally resonant surface waves in a circular cylinder. *J. Fluid Mech.* **149**, 1–14.

Miles, J. W. 1984*b* Resonantly forced surface waves in a circular cylinder. *J. Fluid Mech.* **149**, 15–31.

Miles, J. W. 1990 Capillary–viscous forcing of surface waves. *J. Fluid Mech.* **219**, 635–646.

Miles, J. W. 1994 Faraday waves: rolls versus squares. *J. Fluid Mech.* **269**, 353–371.

Miles, J. W. & Henderson, D. M. 1998 A note on interior vs. boundary-layer damping of surface waves in a circular cylinder. *J. Fluid Mech.* **364**, 319–323.

Moan, T. & Berge, S. (Eds.) 1997 Report of Committee I.2 'Loads'. In *Proc. 13th Intl Ship and Offshore Structures Congress*, Vol. 1, pp. 59–122. Pergamon.

Moiseyev, N. N. 1958 To the theory of nonlinear oscillations of a limited liquid volume of a liquid. *Prikl. Math. Mech.* **22**, 612–621 (in Russian).

Narimanov, G. S. 1957 Movement of a tank partly filled by a fluid: the taking into account of non-smallness of amplitude. *Prikl. Math. Mech.* **21**, 513–524 (in Russian).

Ockendon, J. R. & Ockendon, H. 1973 Resonant surface waves. *J. Fluid Mech.* **59**, 397–413.

Ockendon, H., Ockendon, J. R. & Johnson, A. D. 1986 Resonant sloshing in shallow water. *J. Fluid Mech.* **167**, 465–479.

https://doi.org/10.1017/S0022112000003311 Published online by Cambridge University Press

Olsen, H. & Johnsen, K. R. 1975 Nonlinear sloshing in rectangular tanks. A pilot study on the applicability of analytical models. *Rep.* 74-72-S, Vol. 2. Det Norske Veritas, Hovik, Norway.

Rognebakke, O. F. 1999 Experiment on surge excited resonant sloshing in a rectangular tank. *Unpublished data.*

Rognebakke, O. F. & Faltinsen, O. M. 2000 Damping of sloshing due to roof impact. *15th Intl Workshop on Water Waves and Floating Bodies. Dan Caesarea Hotel, Israel, 27 Feb–1 March 2000.*

Shemer, L. 1990 On the directly generated resonant standing waves in a rectangular tank. *J. Fluid Mech.* **217**, 143–165.

Solaas F. & Faltinsen O. M. 1997 Combined numerical and analytical solution for sloshing in two-dimensional tanks of general shape. *J. Ship Res.* **41**, 118–129.

Tsai, W.-T., Yue, D. K.-P. & Yip, K. M. K. 1990 Resonantly excited regular and chaotic motions in a rectangular wave tank. *J. Fluid Mech.* **216**, 343–380.

Waterhouse, D. D. 1994 Resonant sloshing near a critical depth. *J. Fluid Mech.* **281**, 313–318.

https://doi.org/10.1017/S0022112000003311 Published online by Cambridge University Press